SECURITY INFORMATION

CONFIDENTIAL

RESTRICTED SECURITY INFORMATION

Copy 333
RM L52H19

NACA RM L52H19

NACA

RESEARCH MEMORANDUM

CLASSIFICATION CHANGED TO RESTRICTED
AUTHORITY H.L. DRYDEN CHANGE #1533
DATE 6-11-53 T.C. FRASER, JR.

INVESTIGATION AT LOW SPEED OF THE DOWNWASH, SIDEWASH, AND WAKE CHARACTERISTICS BEHIND A LARGE-SCALE TRIANGULAR WING, INCLUDING THE EFFECTS OF YAW, FULL-SPAN TRAILING-EDGE FLAPS, AND TWO LEADING-EDGE MODIFICATIONS

By Edward F. Whittle, Jr. and John G. Hawes

Langley Aeronautical Laboratory
Langley Field, Va.

CLASSIFICATION CHANGED TO
UNCLASSIFIED
AUTHORITY CROWLEY CHANGE #1775
DATE 12-11-53 T.C.F.

CLASSIFIED DOCUMENT

This material contains information affecting the National Defense of the United States within the meaning of the espionage laws, Title 18, U.S.C., Secs. 793 and 794, the transmission or revelation of which in any manner to unauthorized person is prohibited by law.

NATIONAL ADVISORY COMMITTEE FOR AERONAUTICS

WASHINGTON

October 27, 1952

RESTRICTED SECURITY INFORMATION

CONFIDENTIAL

RESTRICTED
SECURITY INFORMATION

NATIONAL ADVISORY COMMITTEE FOR AERONAUTICS

RESEARCH MEMORANDUM

INVESTIGATION AT LOW SPEED OF THE DOWNWASH, SIDEWASH, AND WAKE CHARACTERISTICS BEHIND A LARGE-SCALE TRIANGULAR WING, INCLUDING THE EFFECTS OF YAW, FULL-SPAN TRAILING-EDGE FLAPS, AND TWO LEADING-EDGE MODIFICATIONS

By Edward F. Whittle, Jr. and John G. Hawes

SUMMARY

An investigation has been made at low speed in the Langley full-scale tunnel of the downwash, sidewash, and wake behind a large-scale 60° triangular wing having 10-percent-thick biconvex airfoil sections. The investigation included the effects on the air-flow characteristics of yawing 10°, deflecting full-span plain flaps 20°, and increasing the leading-edge radius by the addition of nose gloves having the NACA $65_{(06)}$-006.5 and the NACA 65-010 airfoil sections.

The main trailing vortex behind the sharp-edged basic wing is graphically shown to move inboard and to rise farther above the wing-chord plane extended with increasing angle of attack. When the wing was yawed 10°, the vortex on the advanced (left) semispan was enlarged and moved farther inboard while the vortex on the retarded (right) semispan was reduced in size and remained close to the wing tip with increasing angle of attack. As compared with the basic wing at the same lift coefficient, the trailing vortex was smaller and not spread out as much for the wing with full-span flaps deflected 20° and the wake was lower.

The addition of nose gloves having the NACA $65_{(06)}$-006.5 and the NACA 65-010 airfoil sections delayed the formation of the trailing vortex with increasing angle of attack, with the larger-radius glove providing the greatest delay. After the trailing vortex was formed, however, it moved inboard at a faster rate than on the sharp-edged basic wing.

Calculations based on downwash and wake measurements indicate that, for an all-movable horizontal tail having a tail length of about 1.4 times the mean aerodynamic chord of the wing and used in conjunction with a 60° triangular wing, a location at or near the wing-chord plane extended

and a tail area from 0.1 to 0.2 times the wing area would provide more acceptable static longitudinal stability and trim characteristics than other tail locations and tail areas for which calculations were made.

INTRODUCTION

The results of a number of low-speed investigations of triangular-wing characteristics have been published (refs. 1 to 9), but there are few sources of data on the downwash, sidewash, and wake behind full-scale triangular wings. In order to add to the quantitative knowledge of the flow field behind triangular wings, extensive surveys were made behind the 60° triangular wing of references 1 to 3 as part of a general program to investigate full-scale triangular-wing characteristics. These surveys included measurements made behind the sharp-edged basic wing, the wing with full-span plain flaps deflected 20°, the wing yawed 10°, and the wing with the leading edge modified by the addition of two nose gloves having the NACA $65_{(06)}$-006.5 and the NACA 65-010 airfoil sections. The surveys were made in the Langley full-scale tunnel at a Reynolds number of 6.0×10^{6}, corresponding to a Mach number of about 0.07.

Since the completion of this test program, published experimental results have shown that the trailing-edge flaps of a triangular wing may be used to advantage as a lift-producing device (ref. 10). For trim, then, the large pitching-moment coefficients of the triangular wing indicate the use of an all-movable horizontal tail. By assuming the sharp-edged 45° sweptback wing of reference 11 to be an all-movable horizontal tail, some calculations based on the surveys behind the sharp-edged basic 60° triangular wing were made to show important trends of the static longitudinal stability and trim characteristics of an assumed 60° triangular-wing airplane.

COEFFICIENTS AND SYMBOLS

C_L lift coefficient (of wing, unless used with subscript), Lift/q_oS

C_m pitching-moment coefficient about $0.25\bar{c}$ (of wing, unless used with subscript), $\text{Pitching moment}/q_oS\bar{c}$

S area (of wing, unless used with subscript), sq ft

S_t/S ratio of tail area to wing area

c	local chord (of wing, unless used with subscript), ft
$\bar{c}$	mean aerodynamic chord (of wing, unless used with subscript), $\frac{2}{S}\int_0^{b/2} c^2 dy$, ft
b	span (of wing, unless used with subscript), ft
$x/\bar{c}$	static margin $\left(\frac{dC_m}{dC_L} \text{ at } i_t = 0^\circ\right)$ at $C_L = 0$
$\frac{dC_m}{dC_L}$	static longitudinal stability
y	lateral distance from plane of symmetry, ft
z	vertical distance from wing chord plane, positive upward, ft
l	tail length (distance from $0.25\bar{c}$ of wing to $0.25\bar{c}_t$ of tail), ft
q_o	free-stream dynamic pressure, $\frac{1}{2}\rho V^2$, lb/sq ft
q	local-stream dynamic pressure, lb/sq ft
q_t	local dynamic pressure at tail quarter-chord line, lb/sq ft
ρ	mass density of air, slugs/cu ft
V	free-stream velocity, ft/sec
α	angle of attack (of wing, unless used with subscript), deg
i_t	tail incidence angle referred to wing chord line, deg
δ_f	deflection angle of full-span flaps, deg
ϵ	local downwash angle, deg
ψ	yaw angle, deg

Subscripts:

t tail

A airplane

av average value (incremental values taken at tail quarter-chord line)

trim trim condition

MODEL AND APPARATUS

The triangular wing investigated had 60° leading-edge sweep, 10-percent-thick sections, an aspect ratio of 2.31, no geometric twist or dihedral, and the air loads caused no measurable deflection. Three leading-edge configurations were investigated. Configuration A was the original wing having biconvex airfoil sections. Configuration B was obtained by attaching to the leading edge of configuration A a nose glove having the NACA $65_{(06)}$-006.5 airfoil sections faired tangent to the 25-percent-chord line. Configuration C was obtained by attaching to the leading edge of configuration A a nose glove having the NACA 65-010 airfoil sections faired tangent to the 50-percent-chord line. The ordinates and a schematic drawing of these three configurations are presented in table I and figure 1, respectively. A photograph of configuration A is shown in figure 2.

The five-tube survey rake shown in figure 3 was employed to measure the downwash, sidewash, and local dynamic pressures. The rake was calibrated for ±40° of downwash and sidewash. The downwash and sidewash angles are accurate to within about ±0.50° up to angles of about ±20° and to a lesser extent at larger angles. The dynamic-pressure measurements are accurate to within about ±2 percent except at survey locations in the region of low values of dynamic pressure. Because very large values of downwash were expected, the survey rake was given, in some cases, an up-inclination of 15° in order to extend the range of survey data beyond the range of angles for which the rake was calibrated.

The pressures acting on the combined pitch, yaw, and dynamic-pressure tubes were measured on an inclined multiple-tube manometer and photographically recorded.

TESTS AND CORRECTIONS

Configuration A was tested through an angle-of-attack range from about 6° to 28° at yaw angles of 0° and 10° with flaps neutral and through an angle-of-attack range from about 10° to 22° at a yaw angle of 0° with full-span plain flaps deflected 20°. Configurations B and C were tested through an angle-of-attack range from about 11° to 22° at a yaw angle of 0° with flaps neutral.

The surveys were made on the left semispan only except when configuration A was yawed 10°, in which case the surveys covered the full span.

The surveys (fig. 4) were made in 1-foot vertical and horizontal increments in three vertical planes located at $0.53\bar{c}(0.61b/2)$, $1.05\bar{c}(1.21b/2)$, and $1.58\bar{c}(1.82b/2)$ back of the $0.25\bar{c}$ and parallel to the wing trailing edge for the basic wing of configuration A; in two vertical planes located at $0.53\bar{c}$ and $1.05\bar{c}$ for the basic wing of configuration A yawed 10°; and in one vertical plane located at $1.05\bar{c}$ for the wing of configuration A with full-span plain flaps deflected 20°, as well as configurations B and C. When the wing was yawed 10°, the survey planes were also yawed 10° to the same position relative to the wing as for the unyawed case. All tests were made at a Reynolds number of 6.0×10^{6} and a Mach number of approximately 0.07.

The air-stream measurements were corrected for jet-boundary effects and blocking. The jet-boundary effects which consisted of an angle correction to the downwash are given below:

Plane of survey (back of $\bar{c}/4$)	$\Delta\epsilon$, deg	
	$\psi = 0^{\circ}$	$\psi = 10^{\circ}$
$0.53\bar{c}$	$-2.23C_L$	$-2.29C_L$
$1.05\bar{c}$	$-2.64C_L$	$-2.75C_L$
$1.58\bar{c}$	$-2.96C_L$	-------

The jet-boundary effects were calculated by the theoretical methods given in reference 12. The experimental downwash correction data presented in reference 13 indicate that the theoretical jet-boundary correction should be adequate for the range of surveys presented.

A correction for tunnel air-stream misalinement was not applied to the downwash data. These average values were applied to the data,

however, before the static longitudinal stability calculations were made and are included in the results. Average values for each survey plane are given in the following table:

Plane of survey (back of $\bar{c}/4$)	$\Delta\epsilon$, deg
$0.53\bar{c}$	-0.97
$1.05\bar{c}$	-1.16
$1.58\bar{c}$	-1.36

For the cases where the survey rake was given an initial up-inclination of 15°, correction was made so that the downwash was referenced to the horizontal datum plane.

PRESENTATION OF RESULTS

The results of this investigation are presented as follows:

The lift and pitching-moment characteristics of the wing configurations investigated were obtained from the force results of references 2 and 3 and are presented in figure 5. The downwash and sidewash angles are plotted as vectors in order to show clearly the vortex pattern as it developed, with increasing angle of attack, in each survey plane. These vector plots, together with contours of constant dynamic-pressure ratio q/q_o, are presented in figures 6 to 8 for the basic wing of configuration A, figures 9 to 10 for configuration A yawed 10°, figure 11 for configuration A with full-span plain flaps deflected 20°, figure 12 for configuration B, and figure 13 for configuration C. The absence of vectors near the plane of symmetry is due to the physical impossibility of surveying these positions because of the interference of the sting and tail strut with the survey apparatus (fig. 2).

The longitudinal locations of the three assumed tails are shown in figure 14 and the lift curve for the tail, as obtained for the sharp-edged 45° sweptback wing of reference 11, is shown in figure 15. The variation with the wing angle of attack of the average dynamic-pressure ratio $\left(q_t/q_o\right)_{av}$ and the average downwash angle ϵ_{av} is shown in figures 16(a), 16(b), and 16(c) for tail area ratios S_t/S of 0.1, 0.2, and 0.3, respectively. Presented for each tail area ratio is the effect on $\left(q_t/q_o\right)_{av}$ and ϵ_{av} of horizontal-tail heights $2z/b$ of 0.2, 0.3,

and 0.4 for a tail length $l/\bar{c}$ of about 0.7 and horizontal-tail heights $2z/b$ of -0.1, 0.0, 0.1, 0.2, 0.3, and 0.4 for a tail length of about 1.4. The two equations used in determining $\left(q_t/q_o\right)_{av}$ and ϵ_{av} are as follows:

$$\left(q_t/q_o\right)_{av} = \frac{2}{S_t}\int_0^{b_t/2} \frac{q}{q_o}\, c\, dy \tag{1}$$

and

$$\epsilon_{av} = \frac{2}{\left(q_t/q_o\right)_{av} S_t}\int_0^{b_t/2} \frac{q}{q_o}\, c\epsilon\, dy \tag{2}$$

Calculations were made to show the effect of the wake and downwash characteristics on the static longitudinal stability and trim characteristics of the assumed 60° triangular-wing airplane configuration having an all-movable horizontal tail. The results are presented in figure 17 for the same tail area ratios and tail positions presented in figure 16 and for a center-of-gravity location of $0.25\bar{c}$. The pitching-moment and lift coefficients were determined from the following equations:

$$C_{m_A} = C_m - \frac{S_t}{S}\frac{l}{\bar{c}}\left(\frac{q_t}{q_o}\right)_{av} C_{L_t} \tag{3}$$

$$C_{L_A} = C_L + \frac{S_t}{S}\left(\frac{q_t}{q_o}\right)_{av} C_{L_t} \tag{4}$$

where C_{L_t} was obtained from reference 11 for

$$\alpha_t = \alpha - \epsilon_{av} + i_t \tag{5}$$

The effects on the airplane pitching-moment coefficient C_{m_A} (eq. (3)) of change in the moment arm of the tail lift coefficient due to change

in wing angle of attack and tail drag were not included in the calculations; however, sample calculations made for cases that were most likely to have a large effect showed that the pitching-moment coefficients were not appreciably affected except for tail heights of $\frac{2z}{b} = 0.3$ and 0.4 for both the forward and rearward tail locations. The largest effect, of course, was produced for a tail area ratio $\frac{S_t}{S} = 0.3$. But even where the effect was appreciable, the characteristic shape of the curves was not altered.

Since the static margin $x/\bar{c}$ was large in most cases and the trim lift coefficients were low for a center-of-gravity location of $0.25\bar{c}$ (fig. 17), the computations for the more favorable tail heights $\frac{2z}{b} = -0.1$, 0.0, and 0.1 in the rearward location were repeated for center-of-gravity locations corresponding to a more realistic static margin $x/\bar{c}$ of 0.05 at $i_t = 0^{\circ}$. These additional computations, which for completeness also include the effects of tail drag and change in the moment arm of the tail lift coefficient due to change in wing angle of attack, are presented in figure 18.

DISCUSSION

AIR-STREAM SURVEYS

The development of the flow with increasing wing angle of attack has been discussed in detail only for the middle survey plane ($1.05\bar{c}$ back of the wing $\bar{c}/4$). The data for the other two survey planes ($0.53\bar{c}$ and $1.58\bar{c}$ back of the wing $\bar{c}/4$) are presented to indicate the rearward development of the flow field.

Some effort has been made in the present discussion to correlate the observed flow behind the basic wing of configuration A with the measured loading on a similar triangular wing as given in reference 5. The wing of reference 5 had the same plan form and airfoil sections as the present wing but was tested at a much lower Reynolds number. No significant scale effect, however, is to be expected for a sharp-edged wing of this type (ref. 4). The results due to the various configuration changes have been compared with the results obtained for the basic wing of configuration A.

Configuration A

Basic wing.- At an angle of attack of 5.6° (fig. 7(a)), the vortex sheet is clearly evident and is defined approximately by the change in direction of the sidewash component of the flow vectors. The wake is indicated by the low dynamic-pressure contours. The wake center is located approximately on the wing-chord plane extended $\left(\frac{2z}{b} = 0\right)$; but the trailing vortex sheet (indicated by the sharp change in direction of the lateral velocity component) appears to be concentrated slightly above the chord plane extended; that is, the wake and trailing vortex sheet do not quite coincide.

The results of reference 5 show that, at an angle of attack of 4.1°, flow separation had started at the leading edge of the spanwise station $\frac{2y}{b} = 0.916$ and the measured spanwise loading over the outboard stations is somewhat greater than the theoretical spanwise loading.

At an angle of attack of 11.0° (fig. 7(b)), a weak vortex and a small wake concentration are located above the wing tip, but a much stronger vortex and a larger wake concentration are located at $\frac{2y}{b} = 0.75$ and $\frac{2z}{b} = 0.15$. For this case, as shown in reference 5, the leading-edge vortex covers the entire wing chord at about $\frac{2y}{b} = 0.75$ and the remaining tip region, which is essentially immersed in this separated flow, experiences a loss of lift. (It may be noted, however, that the complete stall, as indicated by the tuft studies of refs. 1 and 5, does not occur over this region until a much higher angle of attack is reached.) The strong trailing vortex observed at $\frac{2y}{b} = 0.75$ corresponds to the sharp drop in loading at this point; however, since the strong trailing vortex may be considered, in a sense, as the continuation of the leading-edge separation vortex, it is referred to as the "separation vortex" in the subsequent discussion. The weaker vortex at the tip is referred to as the "tip vortex." It should perhaps be pointed out, with regard to the surveys for $\alpha = 5.6^{\circ}$ (fig. 7(a)), that the low-lift tip area is too small in that case to allow a clear differentiation between the two types of trailing vortices, even though the data of reference 5 indicate a separation vortex along the leading edge for $\alpha = 5.6^{\circ}$.

At $\alpha = 11.0^{\circ}$, the wake center is located slightly above the wing-chord plane extended, and the vortex sheet, which is not so well-defined as it was at $\alpha = 5.6^{\circ}$, again appears to be located slightly above the wake center at the inboard stations.

At the higher angles of attack, the tip vortex is practically no longer in evidence and is presumably wound up in the larger separation vortex. In reference 14, which presents similar surveys for a wing of 45° sweep and having the same sharp-edged airfoil sections, but 0.5 taper ratio (instead of zero taper ratio as for the present triangular wing), the tip vortex was strongly in evidence at the highest angle of attack tested ($\alpha = 18.0^{\circ}$).

At $\alpha = 16.5^{\circ}$ (fig. 7(c)) the separation vortex is larger than at $\alpha = 11.0^{\circ}$ and is located laterally at $\frac{2y}{b} = 0.70$ and vertically at $\frac{2z}{b} = 0.20$. The vortex sheet is not clearly defined. There is no evidence of a definite wake region over the inboard sections because of the outward draining of the low-energy boundary layer from the inboard sections into the separation vortex.

Increasing the angle of attack to 22.1° increased the size of the vortex and caused an upward movement of the vortex center to about $\frac{2z}{b} = 0.30$ but seemed to have little effect on the inboard movement of the vortex center. The location of the vortex sheet is not well-defined and there is no wake observable over the inboard 20 percent of the span. The wake of the separation vortex, however, extends steadily inboard with increasing angle of attack.

At an angle of attack of about 24°, pressure distributions (ref. 5) show flow separation over about the outboard 50 percent of the span. Tuft studies (refs. 1 and 5) indicate complete stall over about the outboard 20 percent of the span.

At an angle of attack of 27.7°, the vortex center moved inboard to about $\frac{2y}{b} = 0.60$ and moved upward to about $\frac{2z}{b} = 0.40$. The vortex wake covered most of the semispan.

Examination of figures 6 to 8 shows that the development of the flow in each plane of survey, with increasing angle of attack, is the same for all three planes of survey. At a given angle of attack, the vortex center moves higher above the wing-chord plane extended as it passes downstream through each plane of survey. Dissipation of the vortex as it passes downstream is indicated by a reduction in the area enclosed by contours of the lower values of q/q_o (0.50 and lower) in the rearmost plane of survey (fig. 8) as compared with the middle plane of survey (fig. 7).

Effect of yawing 10°.- Yawing the basic wing 10° caused an enlargement and a farther inboard movement of the vortex on the advanced (left)

semispan (figs. 9 and 10) as compared with the unyawed wing (figs. 6 and 7) at corresponding angles of attack. The vortex on the retarded (right) semispan, in general, seems to be smaller as compared to the unyawed wing at corresponding angles of attack, and the spanwise location of the vortex core remained close to the wing tip for all angles of attack tested. In general, the span load distribution (ref. 5) shifted inboard, with increasing angle of attack, faster on the advanced (left) semispan and slower on the retarded (right) semispan when compared with the unyawed wing.

Full-span plain flap deflected 20°.- As would be expected with the flap deflected 20°, the entire wake is shifted downward (relative to the original chord plane extended) and the vortex is shifted outboard as compared with the basic wing at equal values of C_L (figs. 7 and 11). At the same time, the size of the vortex is less and not so spread out and the wake is smaller.

Configuration B

The primary effect of rounding the basic-wing leading edge to a radius of approximately 0.0028c by the installation of a nose glove having airfoil ordinates corresponding to the NACA $65_{(06)}$-006.5 airfoil sections appears to be a delay in the formation of the separation vortex (fig. 12). This delay resulted in an improvement in the static longitudinal stability characteristics as seen in figure 5. Although the vortex was delayed in forming on configuration B, its progression inboard with increased angle of attack was faster than for configuration A. The vortex sheet is well-defined at an angle of attack of about 11.0° (fig. 12(a)) though it is not well-defined for configuration A at the same angle of attack (fig. 7(b)).

Configuration C

Increasing the wing leading-edge radius to approximately 0.0069c by installing a nose glove having airfoil ordinates corresponding to the NACA 65-010 airfoil sections delayed the formation of the separation vortex even more than did configuration B and resulted in alleviation of the abrupt force breaks in the longitudinal stability curves characteristic of configuration A and configuration B (fig. 5).

As seen in figure 13(a), the vortex sheet is well-defined and the vortex is weak at an angle of attack of 11.1°, as compared with the sharp-edged basic wing (fig. 7(b)), and is confined to the wing-tip region with the vortex core located at approximately $\frac{2y}{b} = 0.95$. At

an angle of attack of 16.5° (fig. 13(b)), the separation vortex probably exists but has not gained enough strength nor moved far enough inboard to distinguish it from the tip vortex. At the highest angle of attack attained ($\alpha = 22.1^{\circ}$) the separation vortex has spread out and the vortex core is now located at approximately $\frac{2y}{b} = 0.70$.

STABILITY AND TRIM

As previously mentioned, the curves of downwash angle and dynamic-pressure ratio plotted in figure 16 for the basic wing of configuration A represent averages over the areas of the assumed tails. It might be observed that the downwash curves do not all seem to extrapolate to zero downwash angle at zero angle of attack. Part of the difference from zero no doubt results from the inaccuracy of readings. Part of the difference, however, is probably due to the field of the wing, which had an appreciable thickness, and to the inflow into the wing wake; the variation of the discrepancy with tail height roughly correlates with this suggestion.

The curves indicate that the downwash variation with angle of attack is stabilizing $\left(\frac{\partial\epsilon}{\partial\alpha} < 1\right)$ for a range of tail heights $2z/b$ from -0.1 to 0.1 for all tail area ratios S_t/S in the rearward tail location. The higher tail positions, in general, are destabilizing either in the lower or higher angle-of-attack range, in both the tail forward and tail rearward locations.

In general, the variation of $\left(q_t/q_o\right)_{av}$ with angle of attack is unfavorable in the high α range for all tail area ratios S_t/S at $\frac{2z}{b} = 0.2$, 0.3, and 0.4 for both the tail forward and tail rearward locations. The decrease in $\left(q_t/q_o\right)_{av}$ with increasing angle of attack is due to the effect of the wake as the tail passes through the wake with increasing angle of attack.

Since the static margin, in most cases, was large and the trim lift coefficients were low for a center-of-gravity location of $0.25\bar{c}$ (fig. 17) the computations for the more favorable tail heights $\left(\frac{2z}{b} = -0.1\right.$, 0.0, and 0.1) in the rearward tail location were repeated for center-of-gravity locations corresponding to a more realistic static margin $x/\bar{c}$ of 0.05 at $i_t = 0^{\circ}$ (fig. 18). The results show that trim lift

coefficients of about 1.0 were obtained for tail incidence angles of about -8° at a tail height $\frac{2z}{b} = 0$ with values of $\left(\frac{dC_m}{dC_L}\right)_{trim}$ of -0.10 and -0.23 for $\frac{S_t}{S} = 0.1$ and 0.2, respectively. Other tail heights and tail area ratios show either (1) large values of $\left(\frac{dC_m}{dC_L}\right)_{trim}$, (2) maximum $C_{L_{A_{trim}}}$ at rather small negative tail incidence angles, or (3) undesirable reversals in the pitching-moment curves $\left(\text{in particular for } \frac{S_t}{S} = 0.1\right)$. Since a static margin $x/\bar{c}$ of 0.05 at $i_t = 0^{\circ}$ is about the lowest value that will be generally acceptable, not much can be done to reduce large values of $\left(\frac{dC_m}{dC_L}\right)_{trim}$. At the expense of increasing $\left(\frac{dC_m}{dC_L}\right)_{trim}$ somewhat, however, conditions (2) and (3) above can be improved by increasing $x/\bar{c}$ from 0.05 to, say, 0.08 at $i_t = 0^{\circ}$. For a static margin $x/\bar{c}$ of 0.08 at $i_t = 0^{\circ}$, it is expected that the results for $\frac{S_t}{S} = 0.1$ at $\frac{2z}{b} = -0.1$, 0.0, and 0.1 would be the most attractive tail-on configurations.

CONCLUDING REMARKS

An investigation at low speed of the downwash, sidewash, and dynamic-pressure ratio behind a large-scale 60° triangular wing indicates the following conclusions, of which the first two corroborate previous investigations.

1. A separation vortex formed near the apex of the sharp-edged basic wing at a low angle of attack and moved over the wing just behind and parallel to the wing leading edge. It left the wing near the tip and passed downstream. As the angle of attack was increased, the downwash angles and sidewash angles became larger and the dynamic-pressure ratios in the vicinity of the vortex became smaller, while an inboard and upward movement of the vortex occurred relative to the chord plane.

2. The effect of yawing the sharp-edged basic wing 10° primarily was to increase the wing area affected by the vortex on the advanced

semispan because of a broadening of the vortex with increasing angle of attack. The vortex on the retarded semispan moved inboard only slightly with increasing angle of attack.

3. As compared with results for the sharp-edged basic wing at equal values of the lift coefficient C_L, deflecting the full-span flaps 20° delayed the formation and inboard movement of the separation vortex and caused a downward displacement of the wake relative to the chord plane.

4. The addition of a nose glove having NACA $65_{(06)}$-006.5 sections had little effect on the flow characteristics of the basic sharp-edged wing except to cause an initial delay in the formation and inboard movement of the separation vortex.

5. The addition of a nose glove having NACA 65-010 airfoil sections delayed still further the developement of the separation vortex flow over the wing, but, at an angle of attack of about 22°, the flow characteristics were about the same as for the sharp-edged basic wing.

6. The flow surveys behind the wing generally correlated well with the measured pressure distributions and spanwise load distributions on a smaller-scale wing having the same plan form and airfoil sections.

7. Calculations for several tail areas, tail lengths, and tail heights showed that a horizontal all-movable tail having an area ratio S_t/S of 0.1 to 0.2, a tail length of about $1.4\bar{c}$, and a vertical location at or near the wing-chord plane extended would have the more acceptable static longitudinal stability and trim characteristics for the plain 60° triangular-wing configuration investigated.

Langley Aeronautical Laboratory,
National Advisory Committee for Aeronautics,
Langley Field, Va.

REFERENCES

1. Whittle, Edward F, Jr., and Lovell, J. Calvin: Full-Scale Investigation of an Equilateral Triangular Wing Having 10-Percent-Thick Biconvex Airfoil Sections. NACA RM L8G05, 1948.

2. Hawes, John G., and May, Ralph W., Jr.: Investigation at Low Speed of the Effectiveness and Hinge Moments of a Constant-Chord Ailavator on a Large-Scale Triangular Wing With Section Modification. NACA RM L51A26, 1951.

3. McLemore, H. Clyde: Low-Speed Investigation of the Effects of Wing Leading-Edge Modifications and Several Outboard Fin Arrangements on the Static Stability Characteristics of a Large-Scale Triangular Wing. NACA RM L51J05, 1952.

4. Wilson, Herbert A., Jr., and Lovell, J. Calvin: Full-Scale Investigation of the Maximum Lift and Flow Characteristics of an Airplane Having Approximately Triangular Plan Form. NACA RM L6K20, 1947.

5. May, Ralph W., Jr., and Hawes, John G.: Low-Speed Pressure-Distribution and Flow Investigation for a Large Pitch and Yaw Range of Three Low-Aspect-Ratio Pointed Wings Having Leading Edge Swept Back 60° and Biconvex Sections. NACA RM L9J07, 1949.

6. Anderson, Adrien E.: An Investigation at Low Speed of a Large-Scale Triangular Wing of Aspect Ratio Two. II.- The Effect of Airfoil Section Modifications and the Determination of the Wake Downwash. NACA RM A7H28, 1947.

7. Graham, David, and Koenig, David G.: Tests in the Ames 40- by 80-Foot Wind Tunnel of an Airplane Configuration With an Aspect Ratio 2 Triangular Wing and an All-Movable Horizontal Tail — Longitudinal Characteristics. NACA RM A51B21, 1951.

8. Frick, J. P.: Downwash and Total-Head Survey Behind a 60° Delta Wing Model in Incompressible Flow. Report ZA-198, Consolidated Vultee Aircraft Corp., Aug. 25, 1949.

9. Jaquet, Byron M.: Effects of Horizontal-Tail Position, Area, and Aspect Ratio on Low-Speed Static Longitudinal Stability and Control Characteristics of a 60° Triangular-Wing Model Having Various Triangular-All-Movable Horizontal Tails. NACA RM L51I06, 1951.

10. MacLeod, Richard G.: A Preliminary Low-Speed Wind-Tunnel Investigation of a Thin Delta Wing Equipped With a Double and a Single Slotted Flap. NACA RM L51J26, 1952.

11. Proterra, Anthony J.: Aerodynamic Characteristics of a 45° Swept-Back Wing With Aspect Ratio of 3.5 and NACA 2S-50(05)-50(05) Airfoil Sections. NACA RM L7C11, 1947.

12. Katzoff, S., and Hannah, Margery E.: Calculation of Tunnel-Induced Upwash Velocities for Swept and Yawed Wings. NACA TN 1748, 1948.

13. Silverstein, Abe, and Katzoff, S.: Experimental Investigation of Wind-Tunnel Interference on the Downwash Behind an Airfoil. NACA Rep. 609, 1937.

14. Lange, Roy H., and Fink, Marvin P.: Studies of the Flow Field Behind a Large-Scale 47.5° Sweptback Wing Having Circular-Arc Airfoil Sections and Equipped With Drooped-Nose and Plain Flaps. NACA RM L51L12, 1952.

TABLE I.- AIRFOIL ORDINATES PARALLEL TO PLANE OF

SYMMETRY OF WING CONFIGURATIONS TESTED

Station (percent c)	Configuration A	Configuration B	Configuration C
	Basic wing (10-percent; circular arc)	Wing with NACA $65_{(06)}$-006.5 glove	Wing with NACA 65-010 glove
	Ordinates (± percent c)	Ordinates (± percent c)	Ordinates (± percent c)
0	----	----	----
.50	----	0.51	0.77
.75	----	.61	.93
1.25	0.25	.77	1.17
2.5	.49	1.03	1.57
5.0	.96	1.42	2.18
7.5	1.40	1.74	2.65
10	1.81	2.05	3.04
15	2.56	2.65	3.66
20	3.21	3.22	4.07
25	3.75	3.75	4.42
30	4.21	4.21	4.67
35	4.55	4.55	4.81
40	4.80	4.80	4.92
45	4.95	4.95	4.98
50	5.00	5.00	5.00
55	4.95	4.95	4.95
60	4.80	4.80	4.80
65	4.55	4.55	4.55
70	4.21	4.21	4.21
75	3.75	3.75	3.75
80	3.21	3.21	3.21
85	2.56	2.56	2.56
90	1.81	1.81	1.81
95	.96	.96	.96
100	----	----	----
		L.E. radius = 0.00282c	L.E. radius = 0.00687c

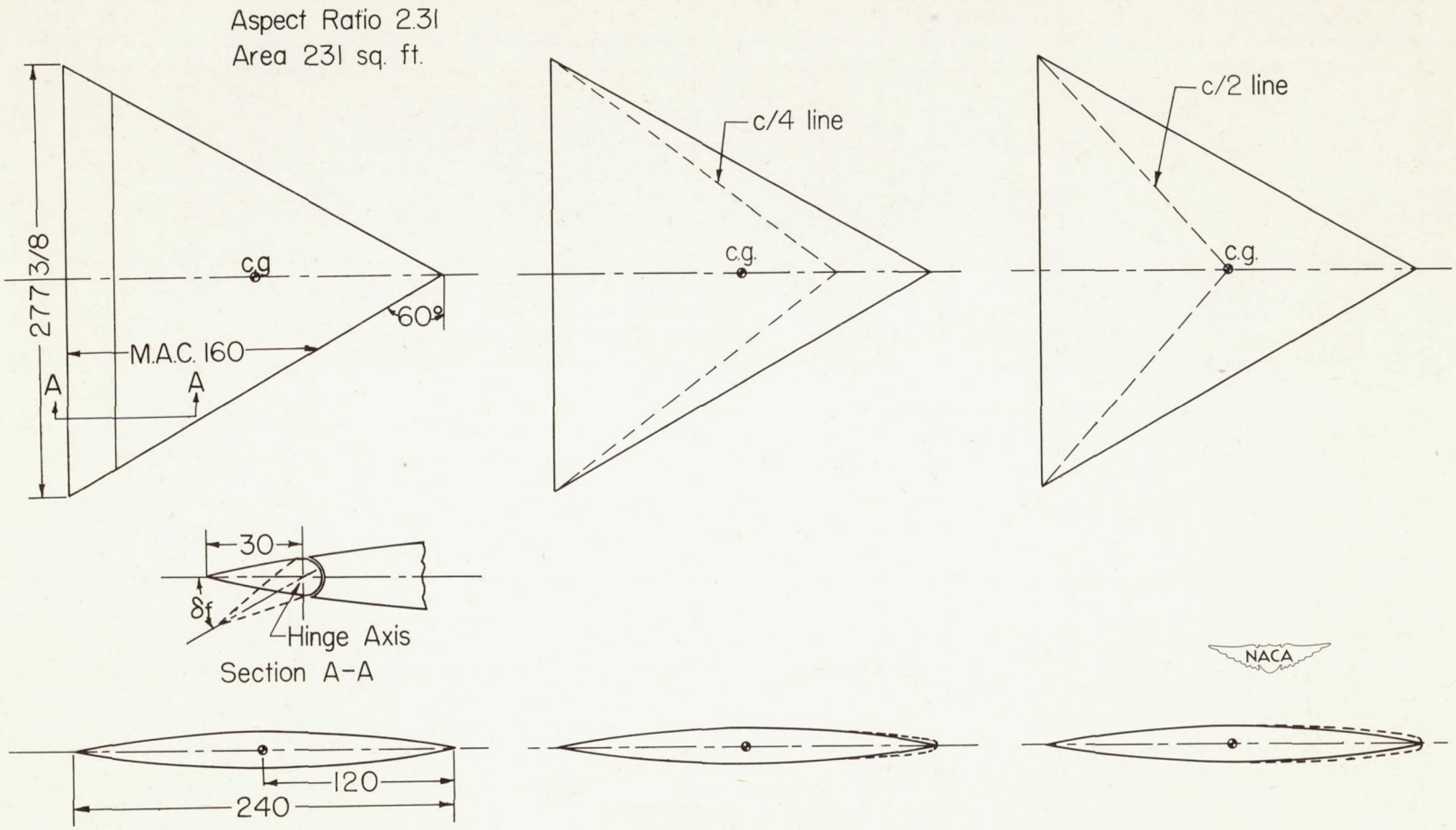

(a) Basic biconvex wing. Configuration A.

(b) Wing with 65-006.5 nose glove. Configuration B.

(c) Wing with 65-010 nose glove. Configuration C.

Figure 1.- Geometric characteristics of basic and nose-glove wing configurations. All dimensions are in inches.

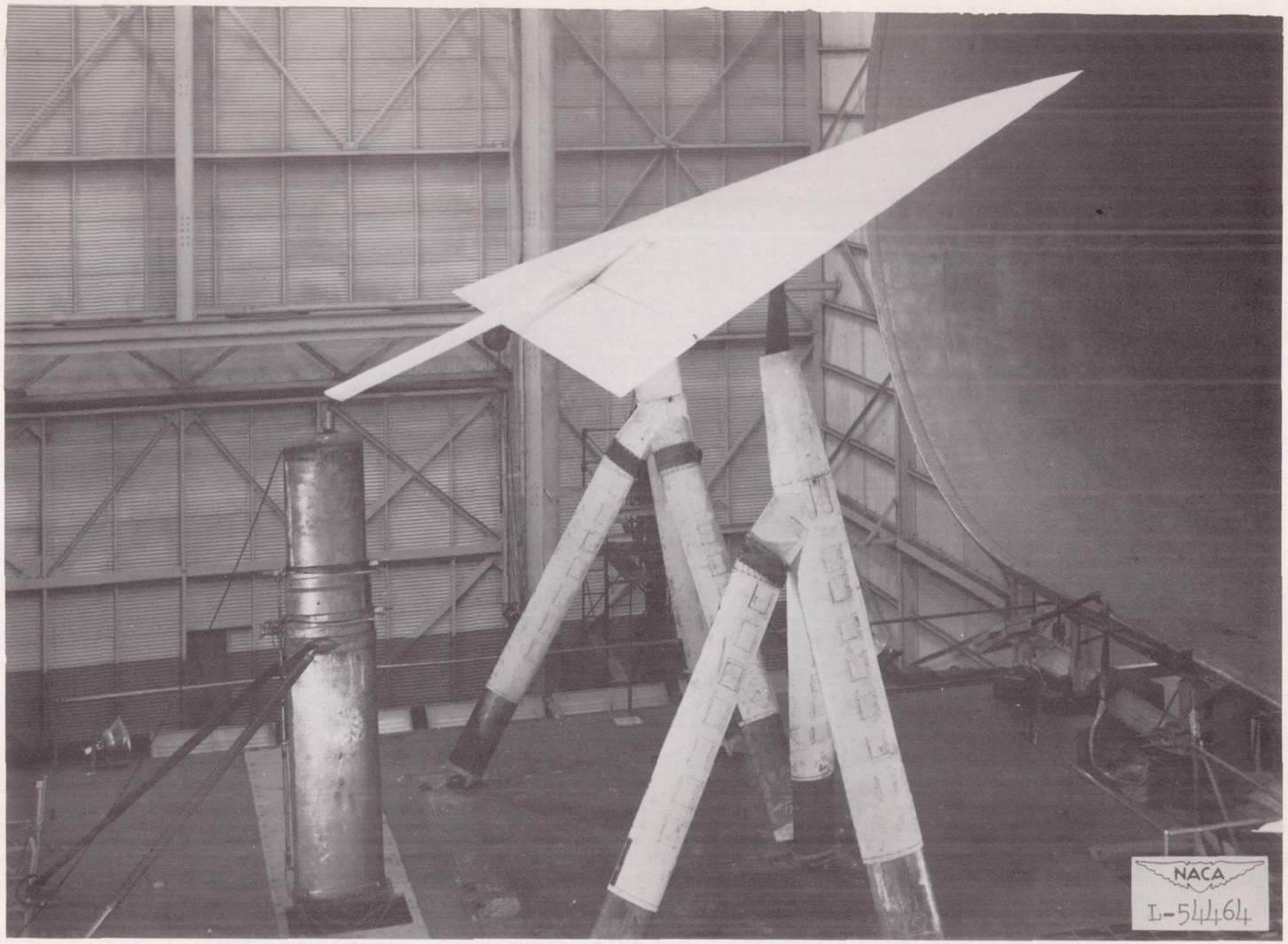

Figure 2.- The basic low-aspect-ratio triangular wing mounted in the Langley full-scale tunnel. Configuration A.

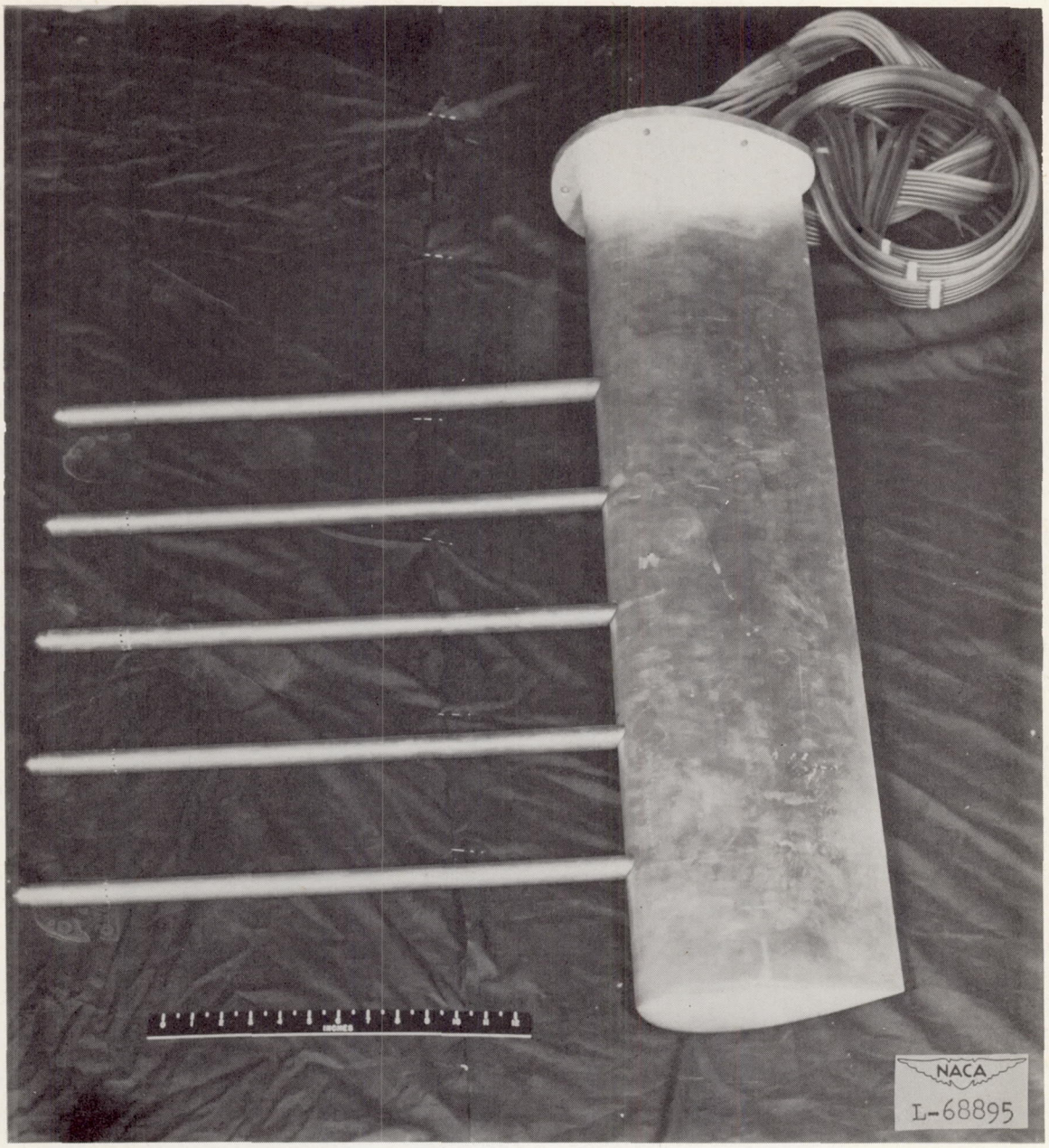

Figure 3.- The five-tube survey rake.

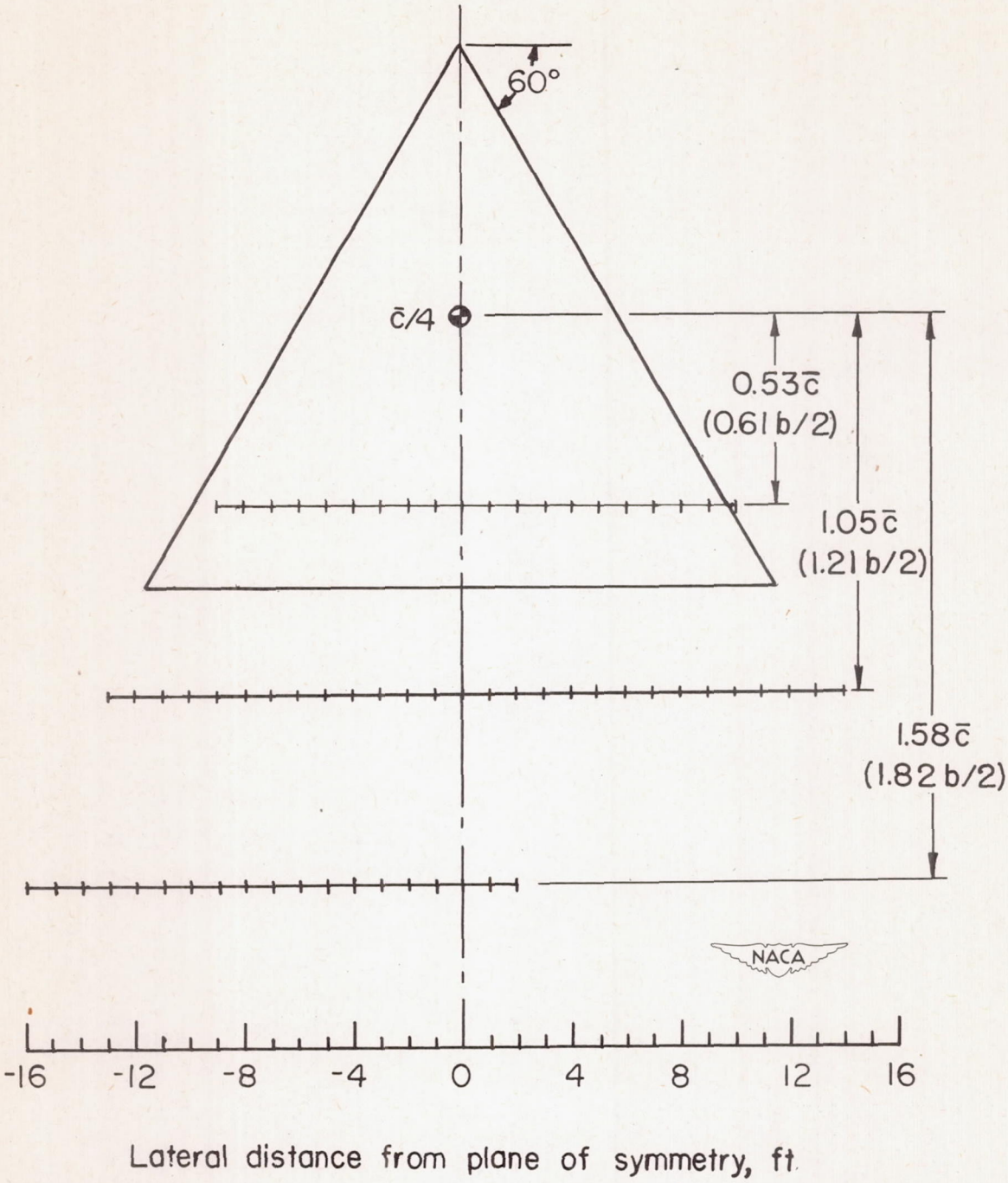

Figure 4.- Longitudinal locations of the three vertical survey planes.

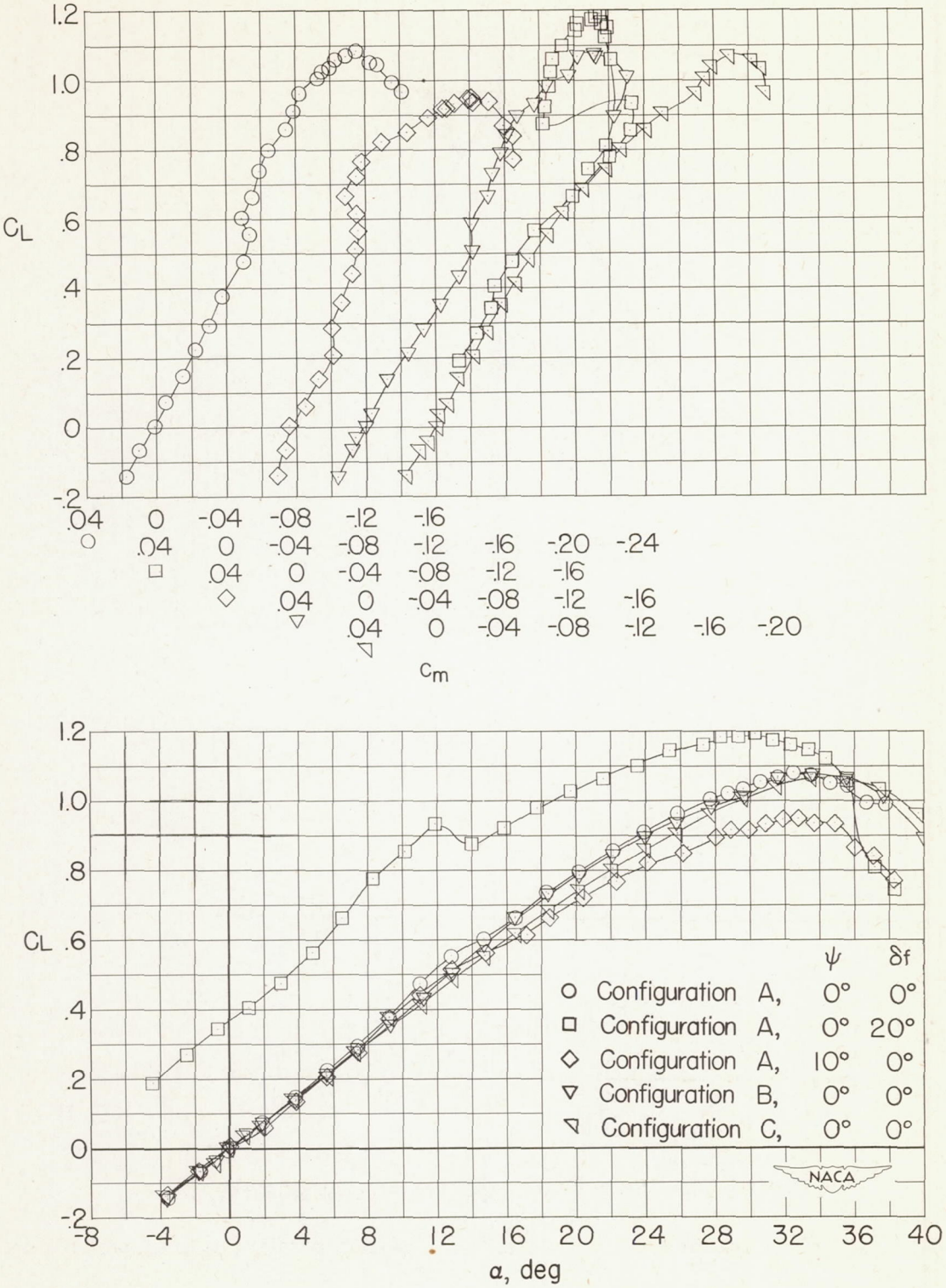

Figure 5.- Lift and pitching-moment characteristics, from force tests, of the configurations for which downwash and sidewash measurements were made.

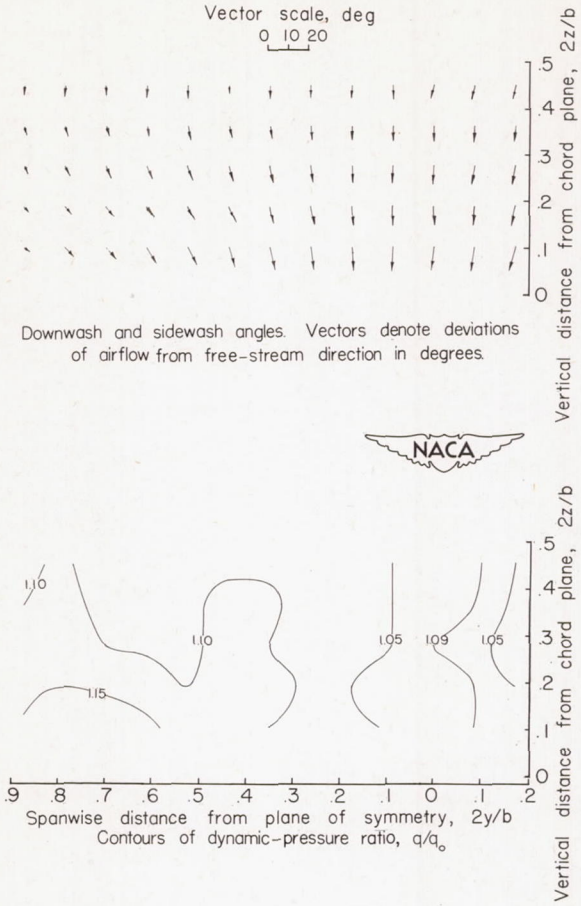

(a) $C_L = 0.22$; $\alpha = 5.6^{\circ}$.

Figure 6.- Vectors of downwash and sidewash and contours of dynamic-pressure ratio above a 60° triangular wing. Longitudinal plane of survey at $0.53\bar{c}$ back of $\bar{c}/4$. Configuration A; $\psi = 0^{\circ}$; $\delta_f = 0^{\circ}$.

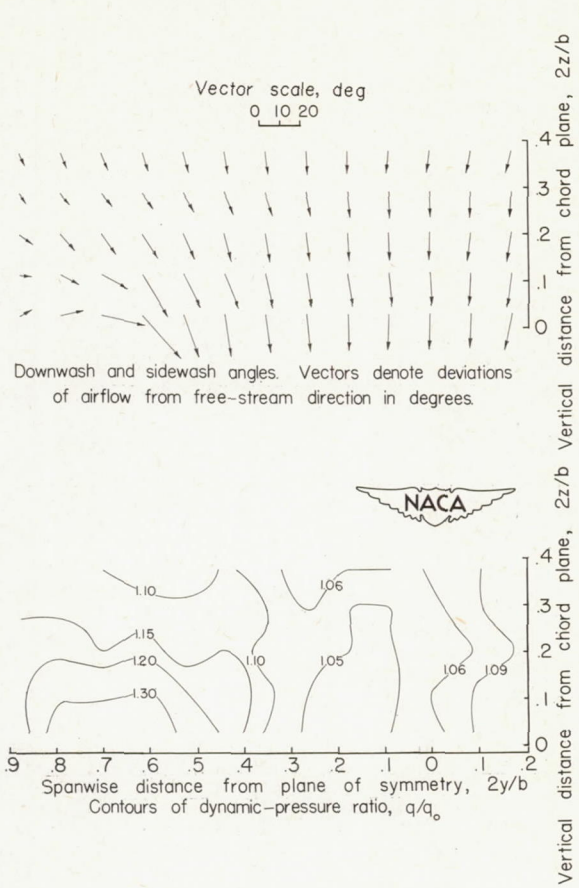

(b) $C_L = 0.47$; $\alpha = 11.0^{\circ}$.

Figure 6.- Continued.

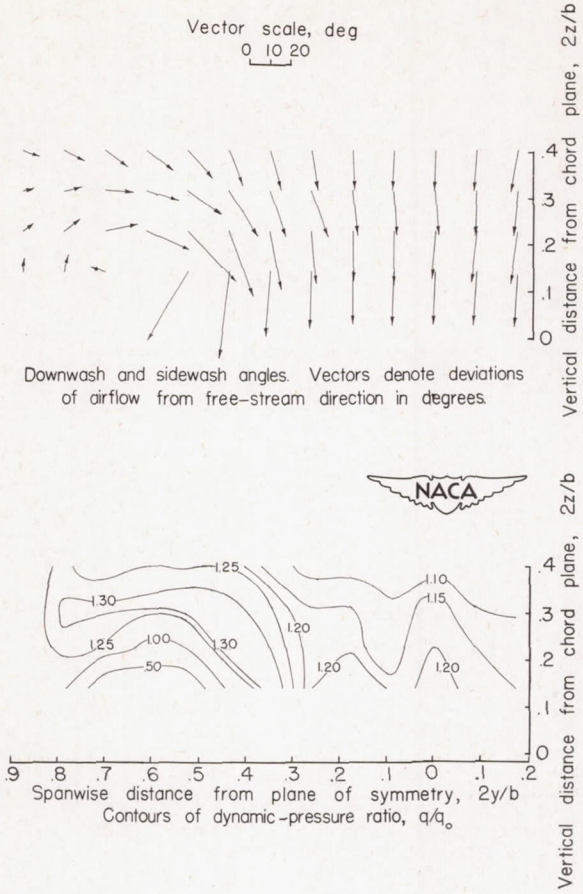

(c) $C_L = 0.66$; $\alpha = 16.5^{\circ}$.

Figure 6.- Continued.

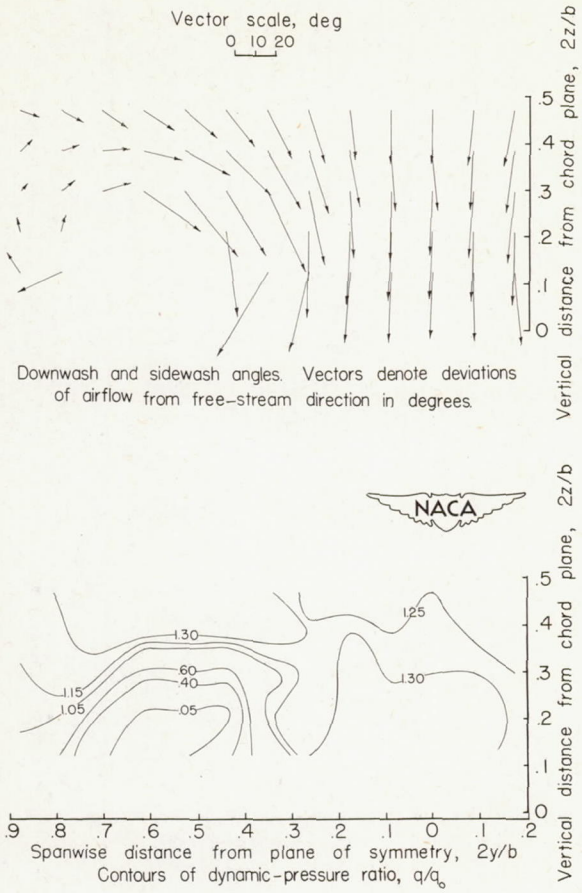

(d) $C_L = 0.86$; $\alpha = 22.1^{\circ}$.

Figure 6.- Continued.

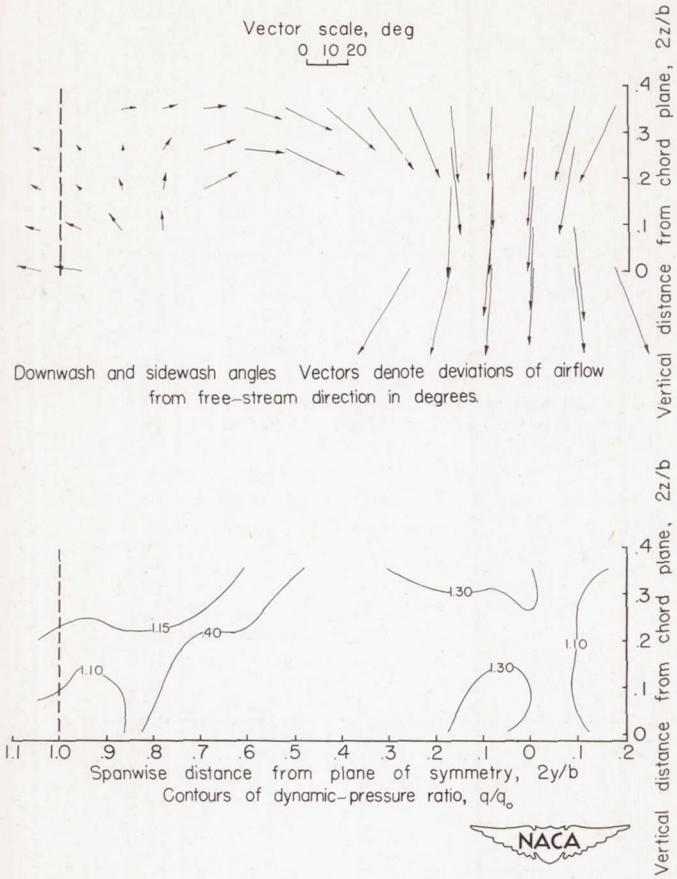

(e) $C_L = 1.01$; $\alpha = 27.7^{\circ}$.

Figure 6.- Concluded.

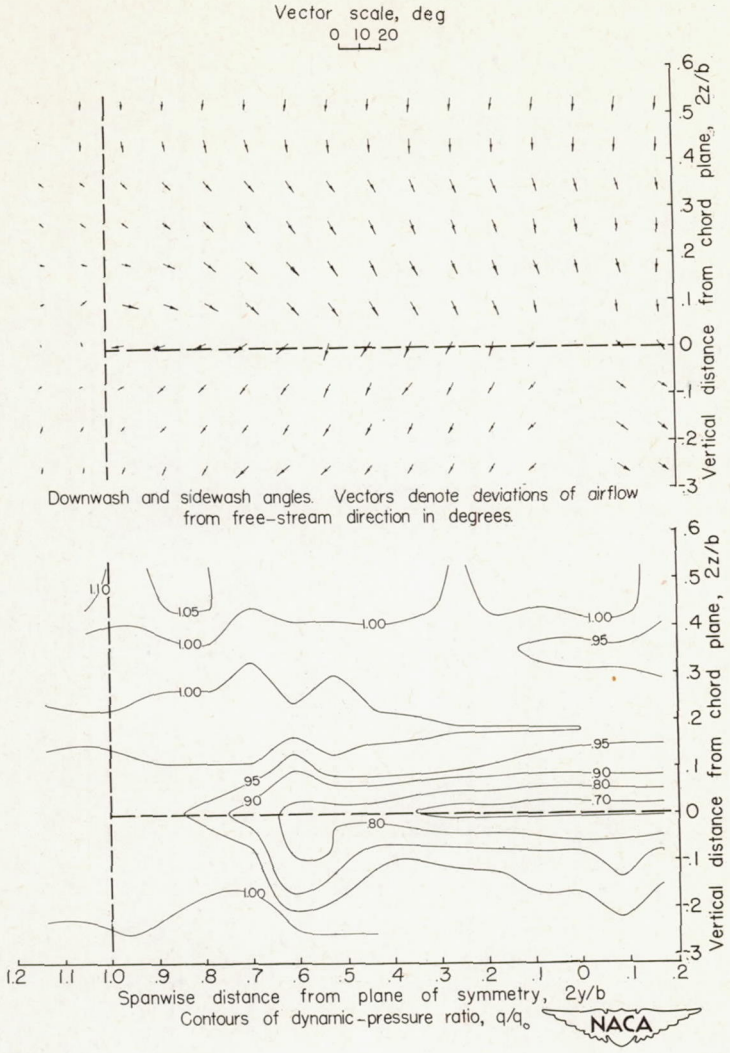

(a) $C_L = 0.22$; $\alpha = 5.6^{\circ}$.

Figure 7.- Vectors of downwash and sidewash and contours of dynamic-pressure ratio behind a 60° triangular wing. Longitudinal plane of survey at $1.05\bar{c}$ back of $\bar{c}/4$. Configuration A; $\psi = 0^{\circ}$; $\delta_f = 0^{\circ}$.

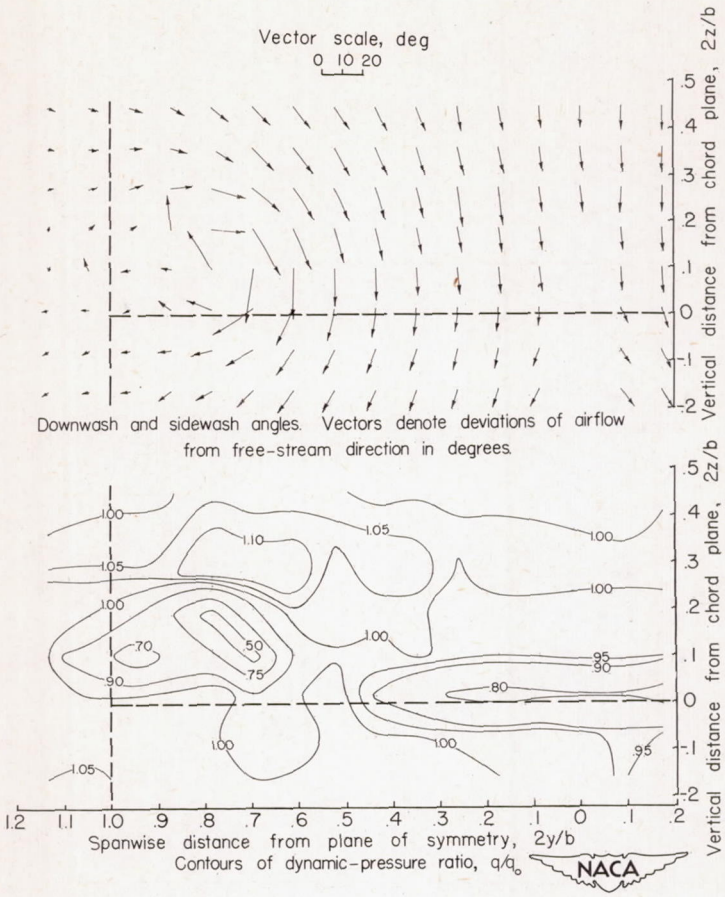

(b) $C_L = 0.47$; $\alpha = 11.0^{\circ}$.

Figure 7.- Continued.

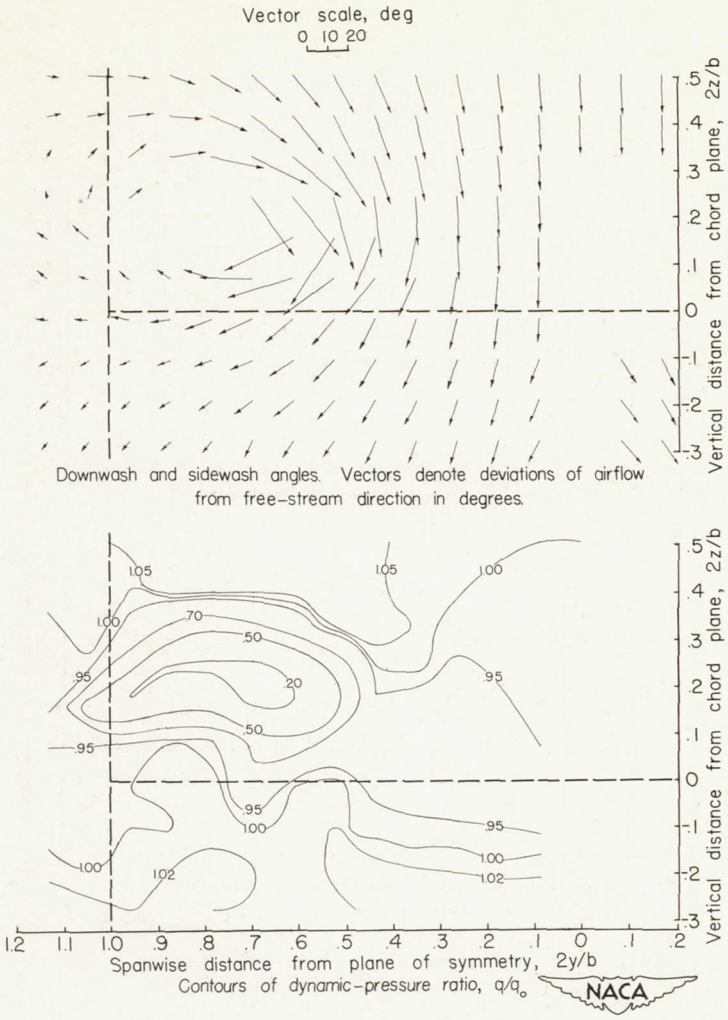

(c) $C_L = 0.66$; $\alpha = 16.5^{\circ}$.

Figure 7.- Continued.

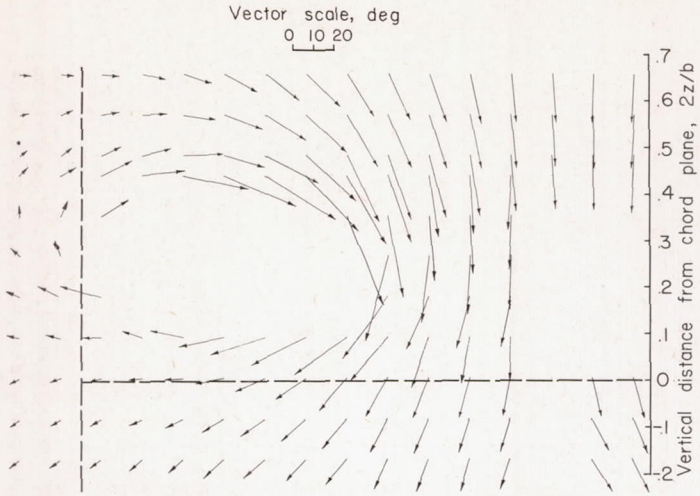

Downwash and sidewash angles. Vectors denote deviations of airflow from free-stream direction in degrees.

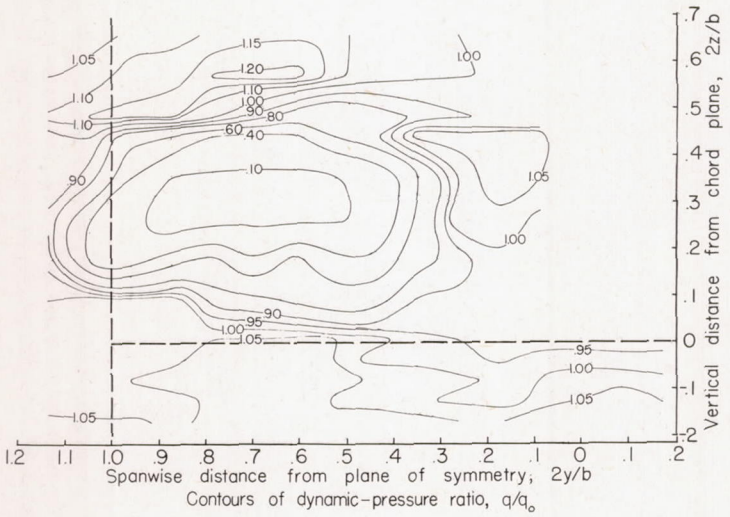

Contours of dynamic-pressure ratio, q/q_o

(d) $C_L = 0.86$; $\alpha = 22.1^{\circ}$.

Figure 7.- Continued.

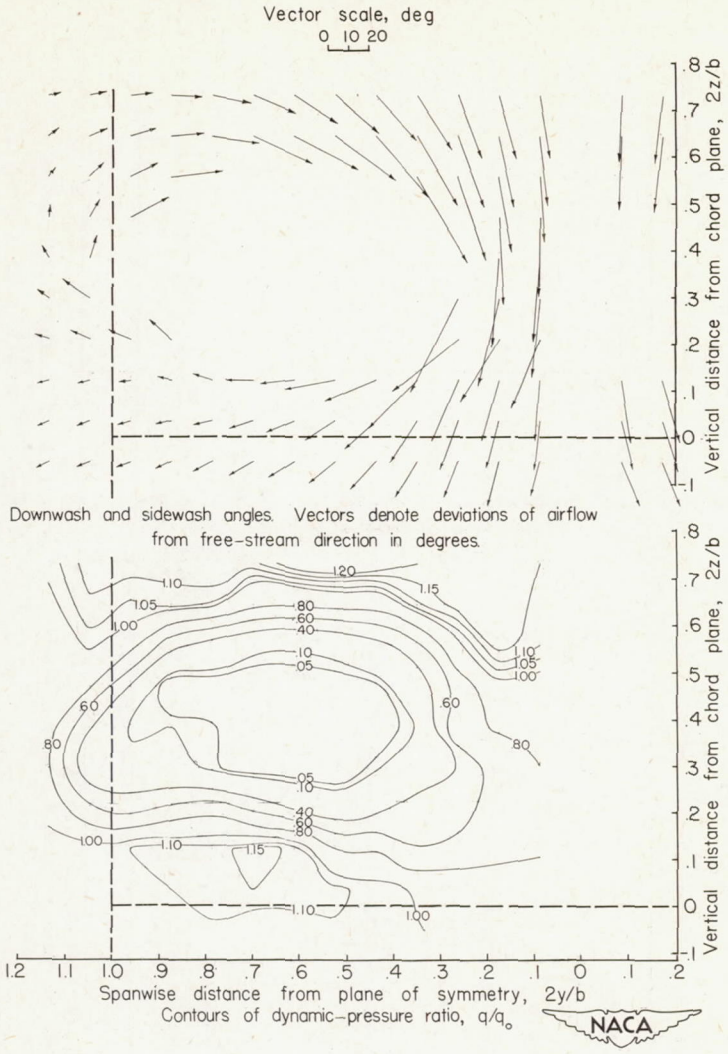

(e) $C_L = 1.01$; $\alpha = 27.7^{\circ}$.

Figure 7.- Concluded.

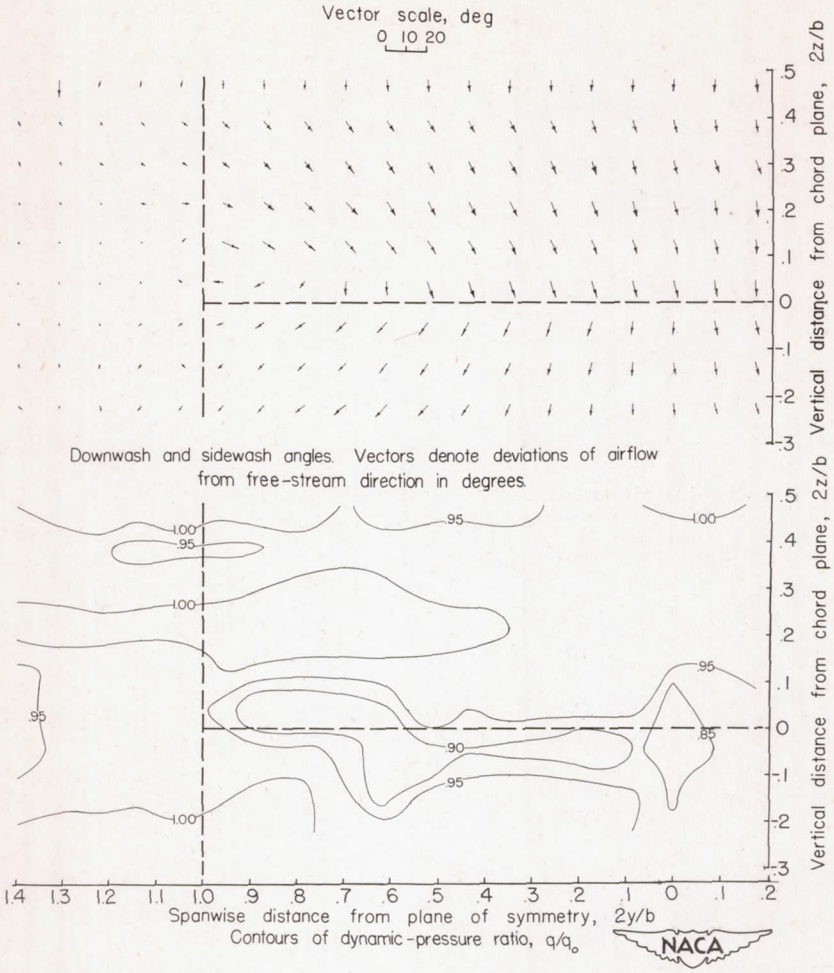

(a) $C_L = 0.22$; $\alpha = 5.6^{\circ}$.

Figure 8.- Vectors of downwash and sidewash and contours of dynamic-pressure ratio behind a 60° triangular wing. Longitudinal plane of survey at $1.58\bar{c}$ back of $\bar{c}/4$. Configuration A; $\psi = 0^{\circ}$; $\delta_f = 0^{\circ}$.

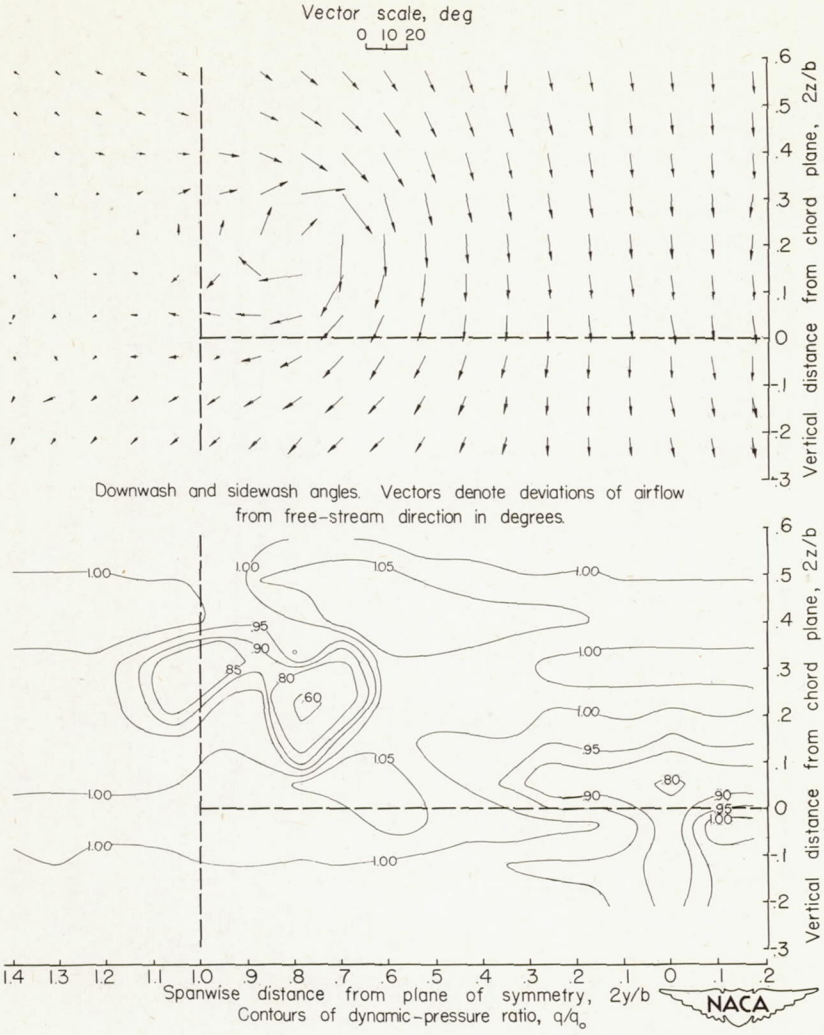

(b) $C_L = 0.47$; $\alpha = 11.0^{\circ}$.

Figure 8.- Continued.

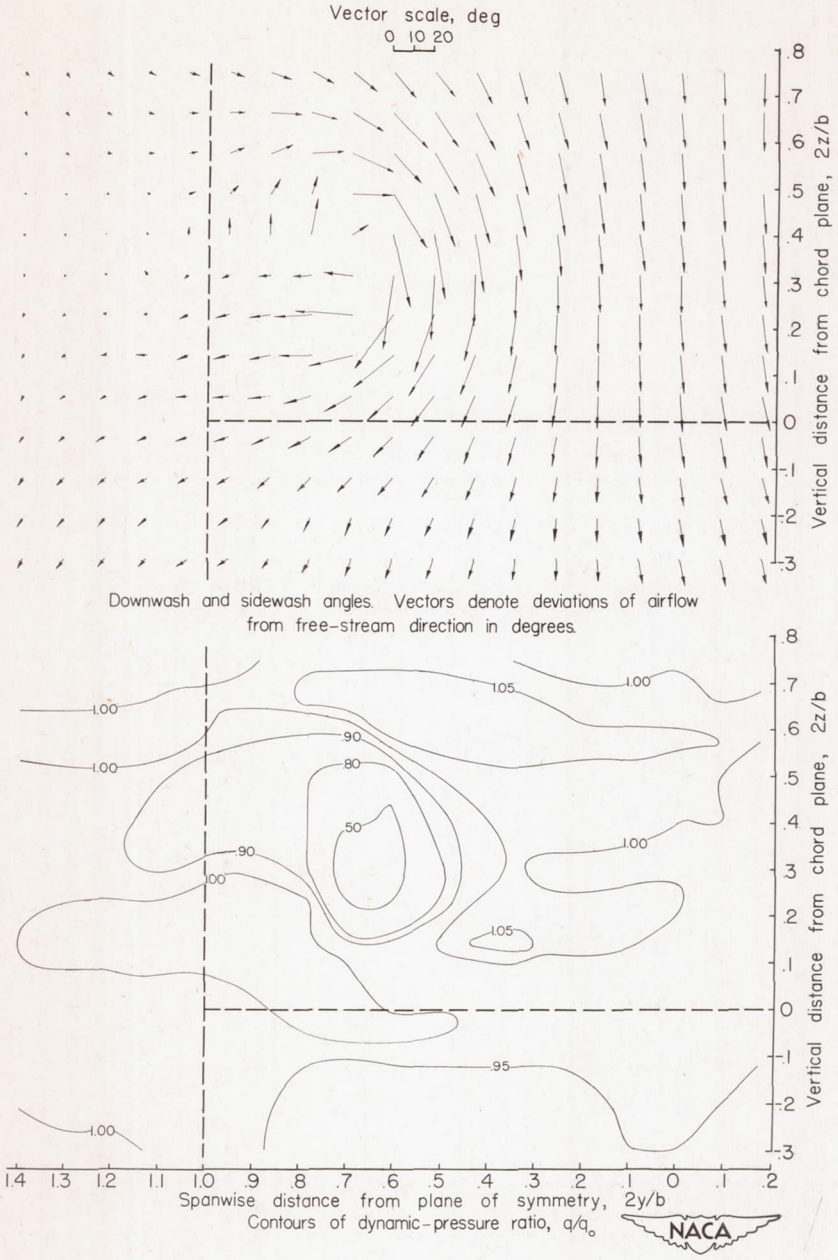

(c) $C_L = 0.66$; $\alpha = 16.5^{\circ}$.

Figure 8.- Continued.

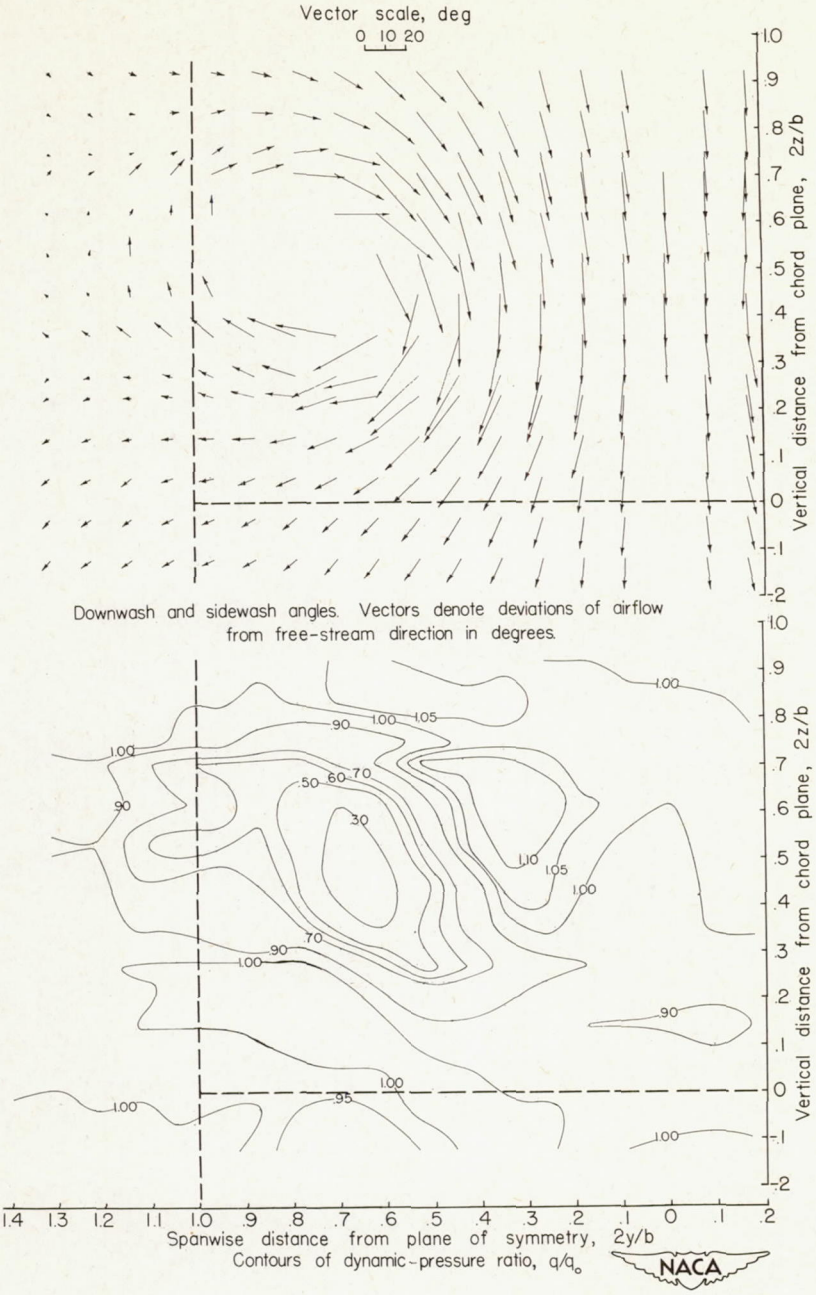

(d) $C_L = 0.86$; $\alpha = 22.1^{\circ}$.

Figure 8.- Continued.

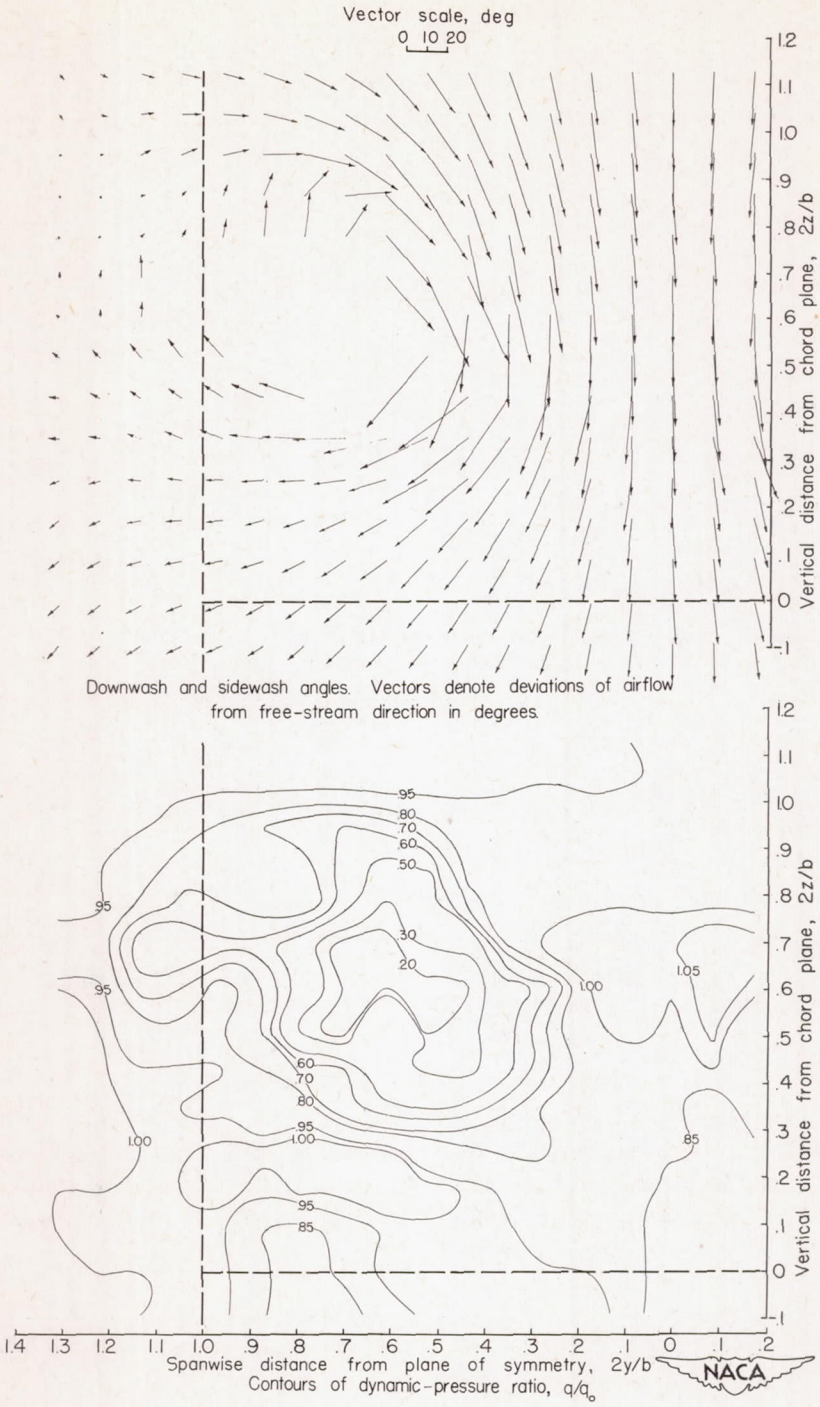

(e) $C_L = 1.01$; $\alpha = 27.7^{\circ}$.

Figure 8.- Concluded.

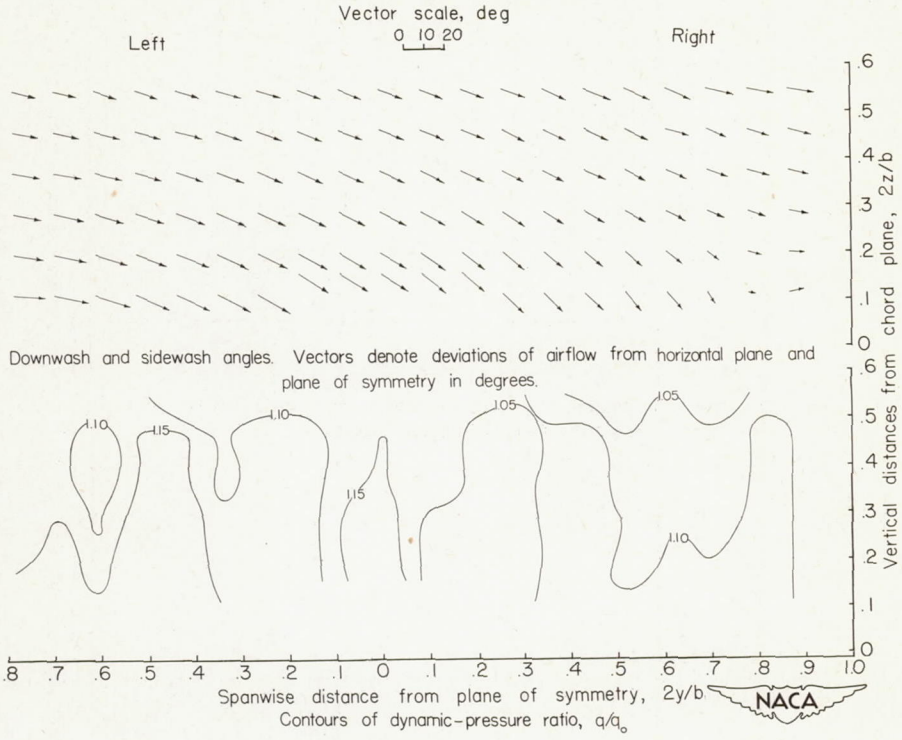

(a) $C_L = 0.21$; $\alpha = 5.6^{\circ}$.

Figure 9.- Vectors of downwash and sidewash and contours of dynamic-pressure ratio above a 60° triangular wing. Longitudinal plane of survey at $0.53\bar{c}$ back of $\bar{c}/4$. Configuration A; $\psi = 10^{\circ}$; $\delta_f = 0^{\circ}$.

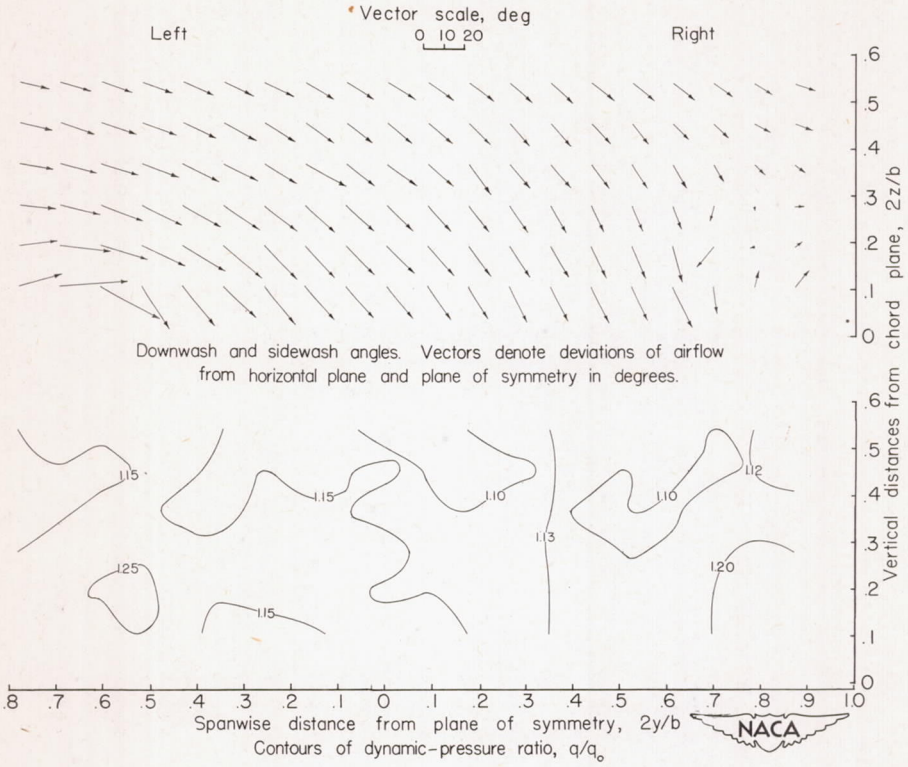

(b) $C_L = 0.43$; $\alpha = 11.0^{\circ}$.

Figure 9.- Continued.

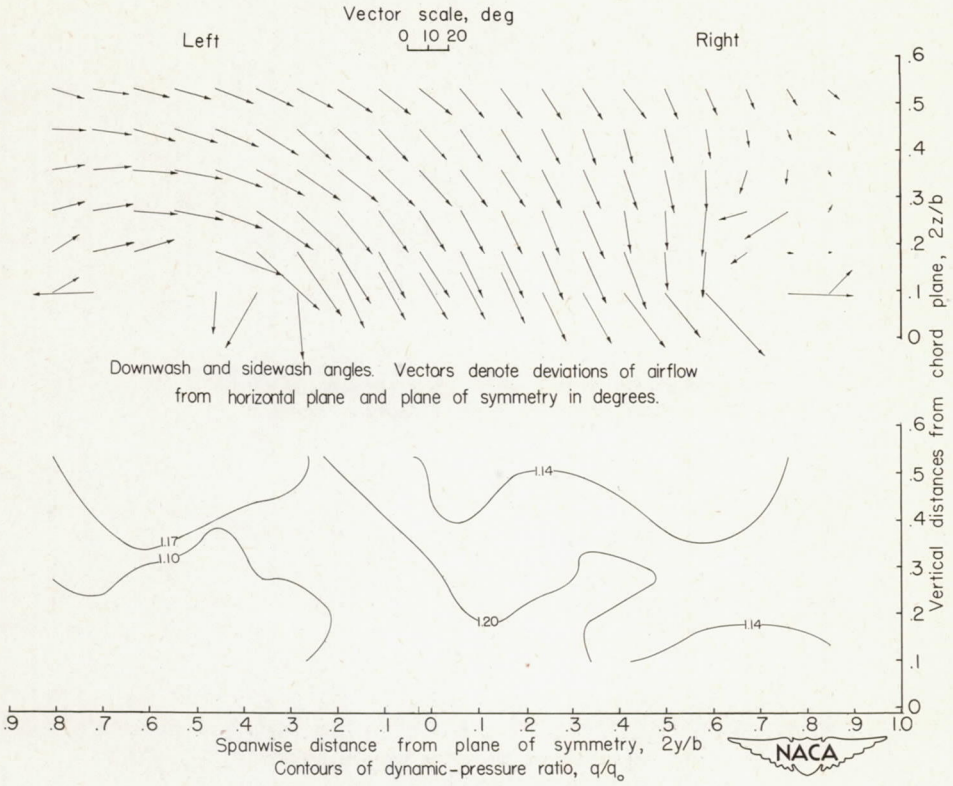

(c) $C_L = 0.62$; $\alpha = 16.6^{\circ}$.

Figure 9.- Continued.

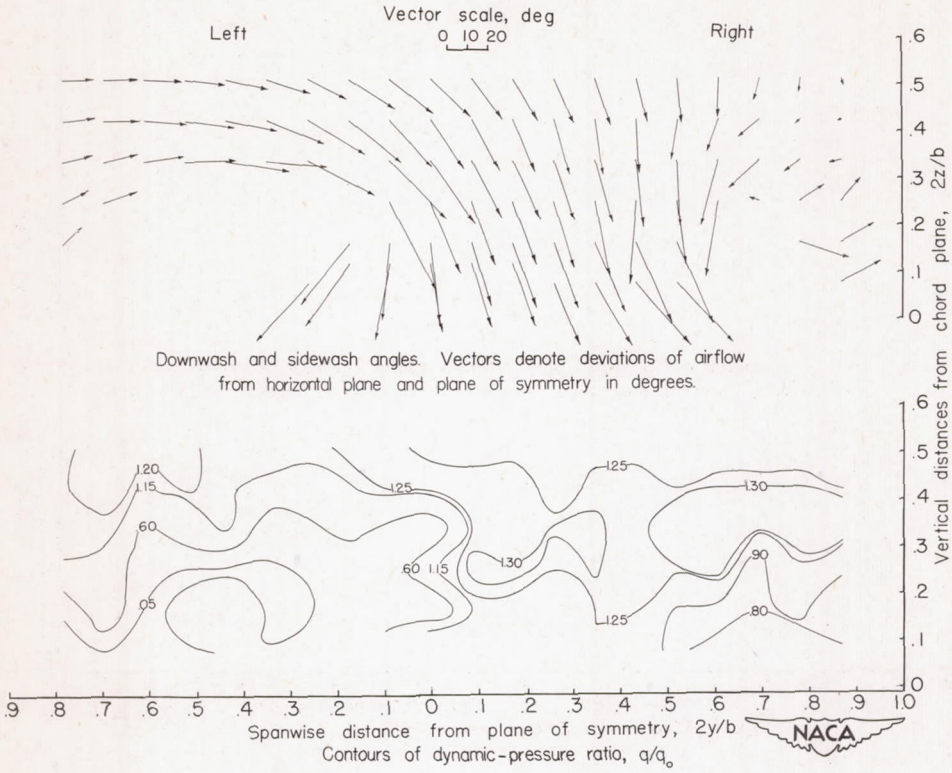

(d) $C_L = 0.77$; $\alpha = 22.3^{\circ}$.

Figure 9.- Continued.

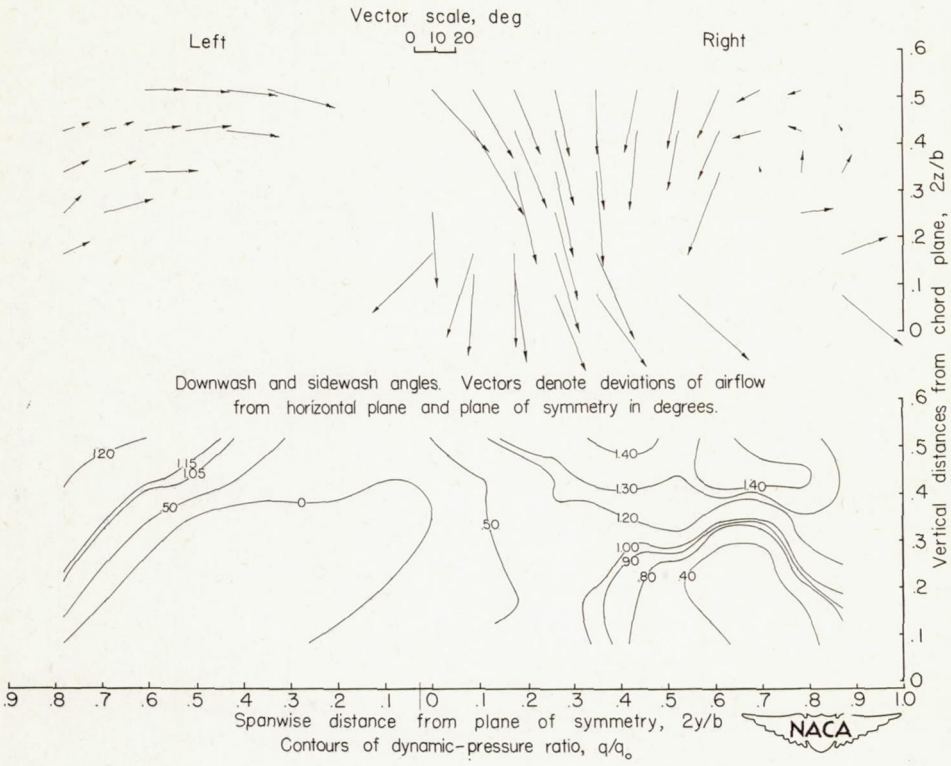

(e) $C_L = 0.90$; $\alpha = 28.0^{\circ}$.

Figure 9.- Concluded.

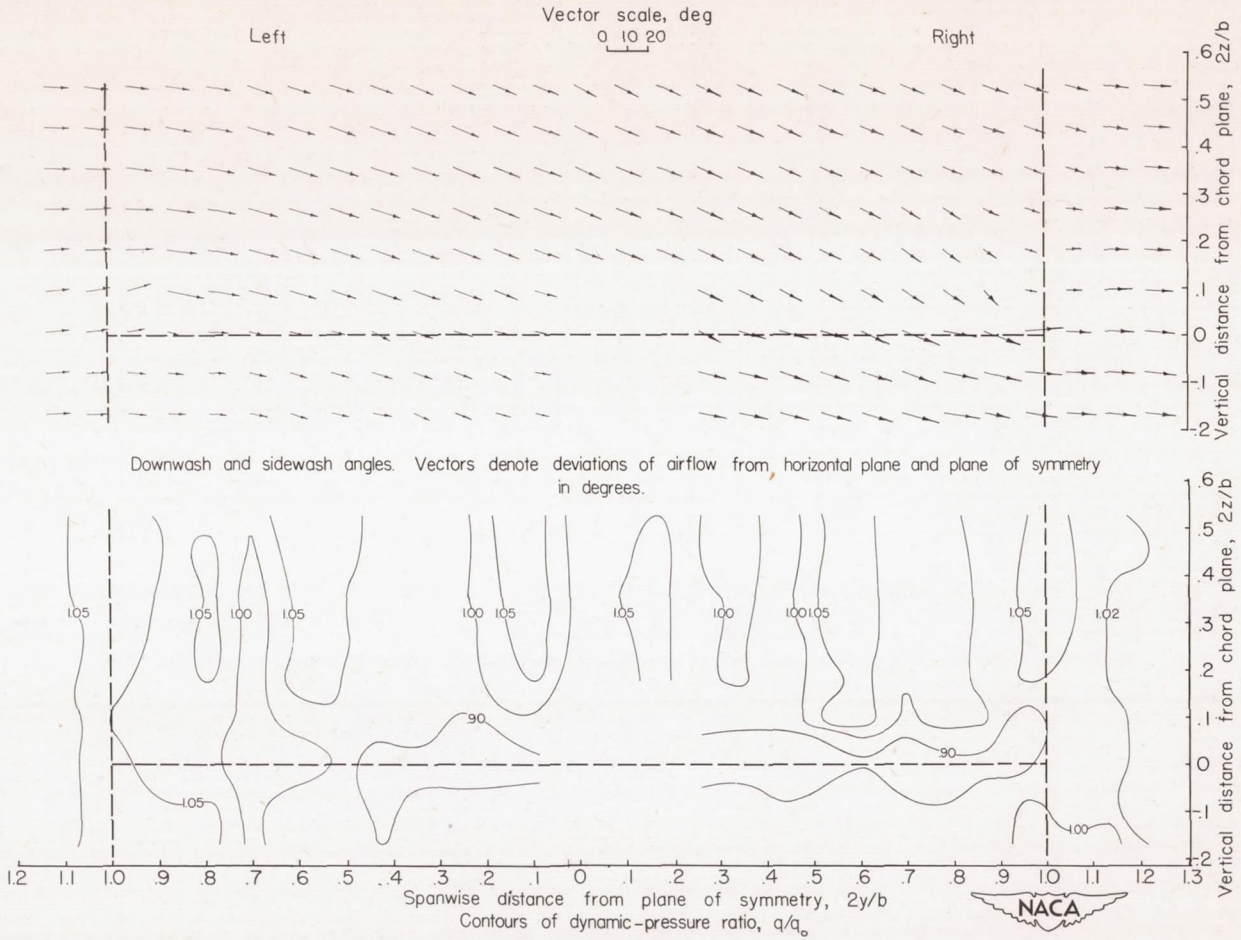

(a) $C_L = 0.21$; $\alpha = 5.6^{\circ}$.

Figure 10.- Vectors of downwash and sidewash and contours of dynamic-pressure ratio above a 60° triangular wing. Longitudinal plane of survey at $1.05\bar{c}$ back of $\bar{c}/4$. Configuration A; $\psi = 10^{\circ}$; $\delta_f = 0^{\circ}$.

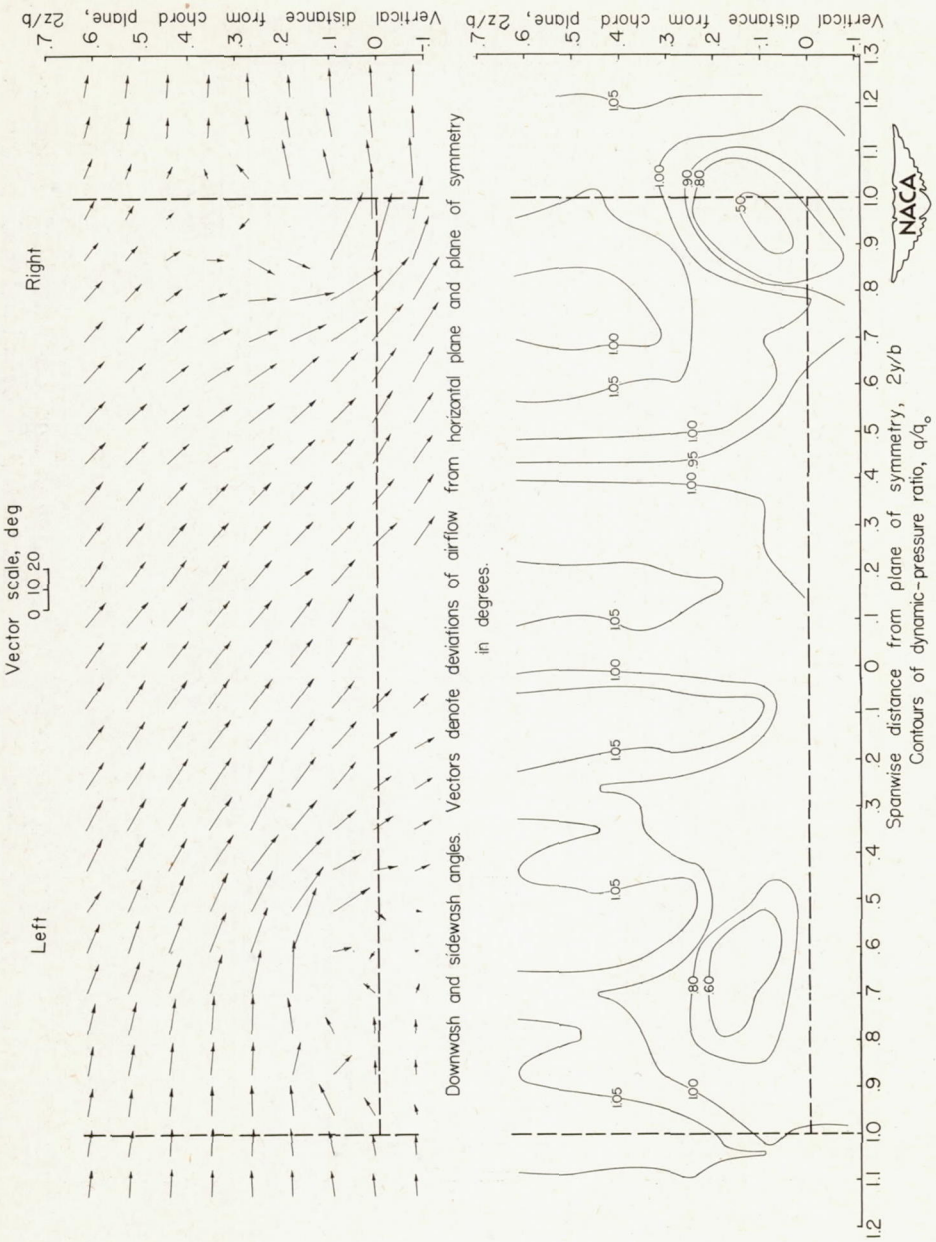

(b) $C_L = 0.44$; $\alpha = 11.0^{\circ}$.

Figure 10.- Continued.

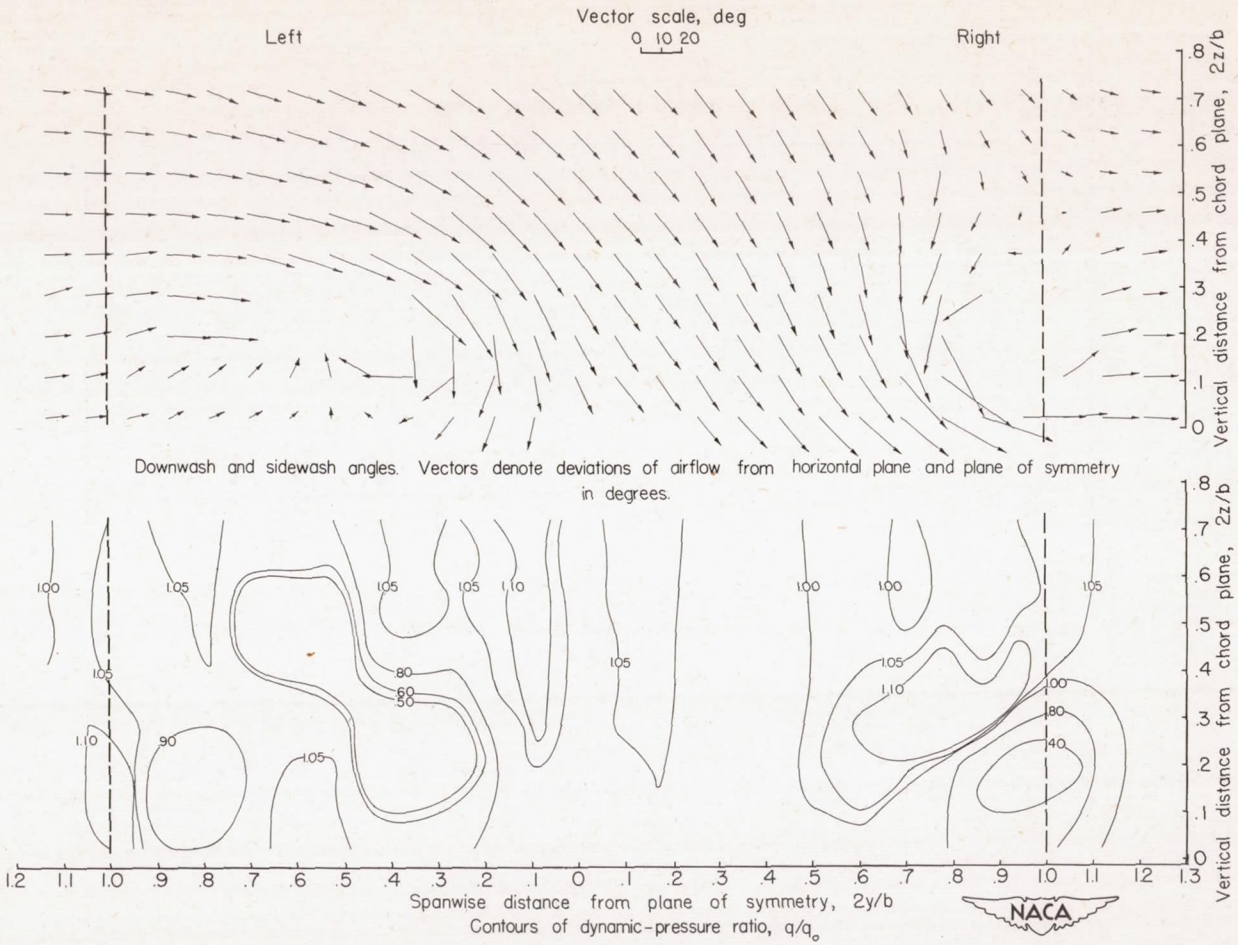

(c) $C_L = 0.62$; $\alpha = 16.6^{\circ}$.

Figure 10.- Continued.

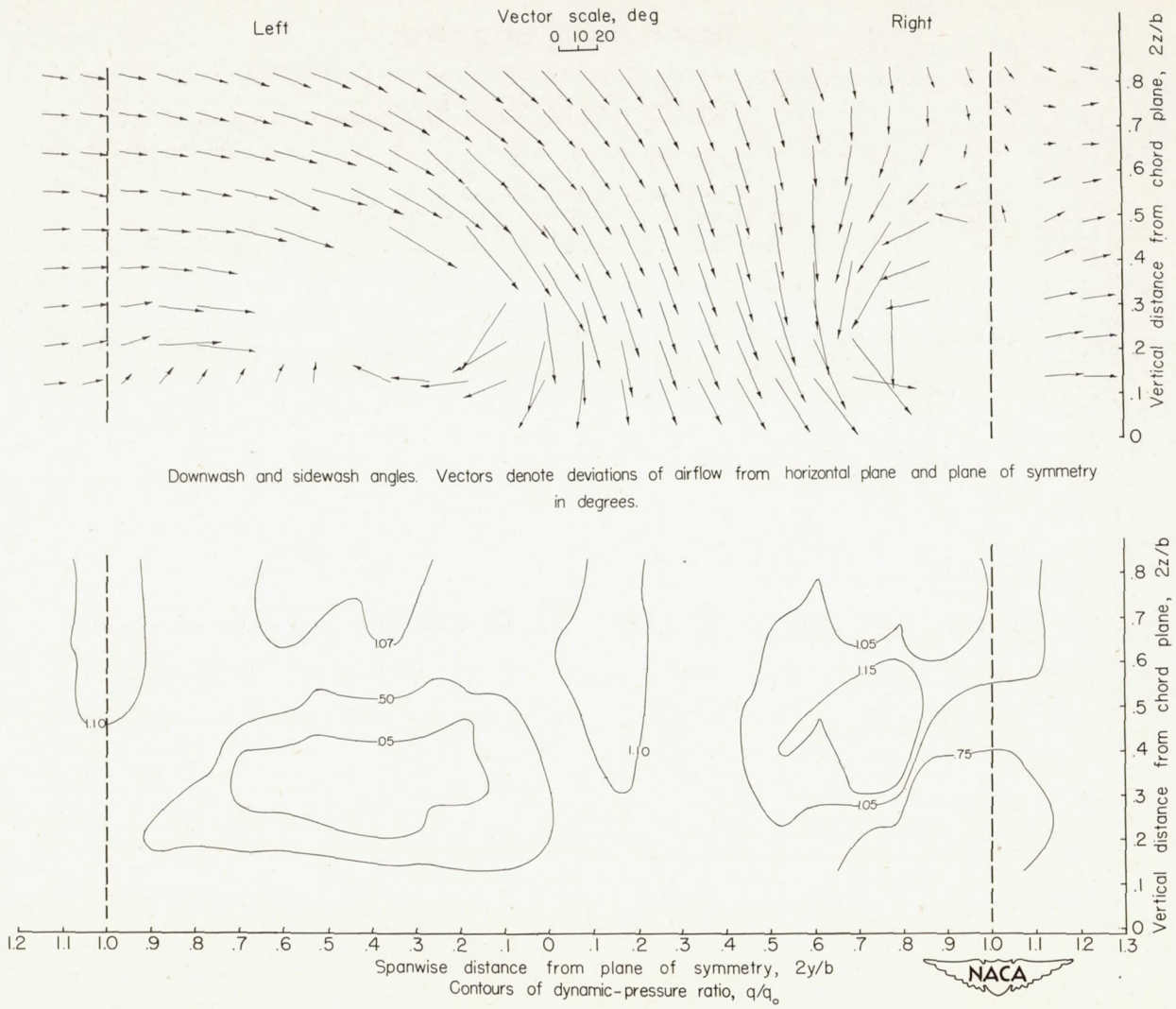

(d) $C_L = 0.77$; $\alpha = 22.3^{\circ}$.

Figure 10.- Continued.

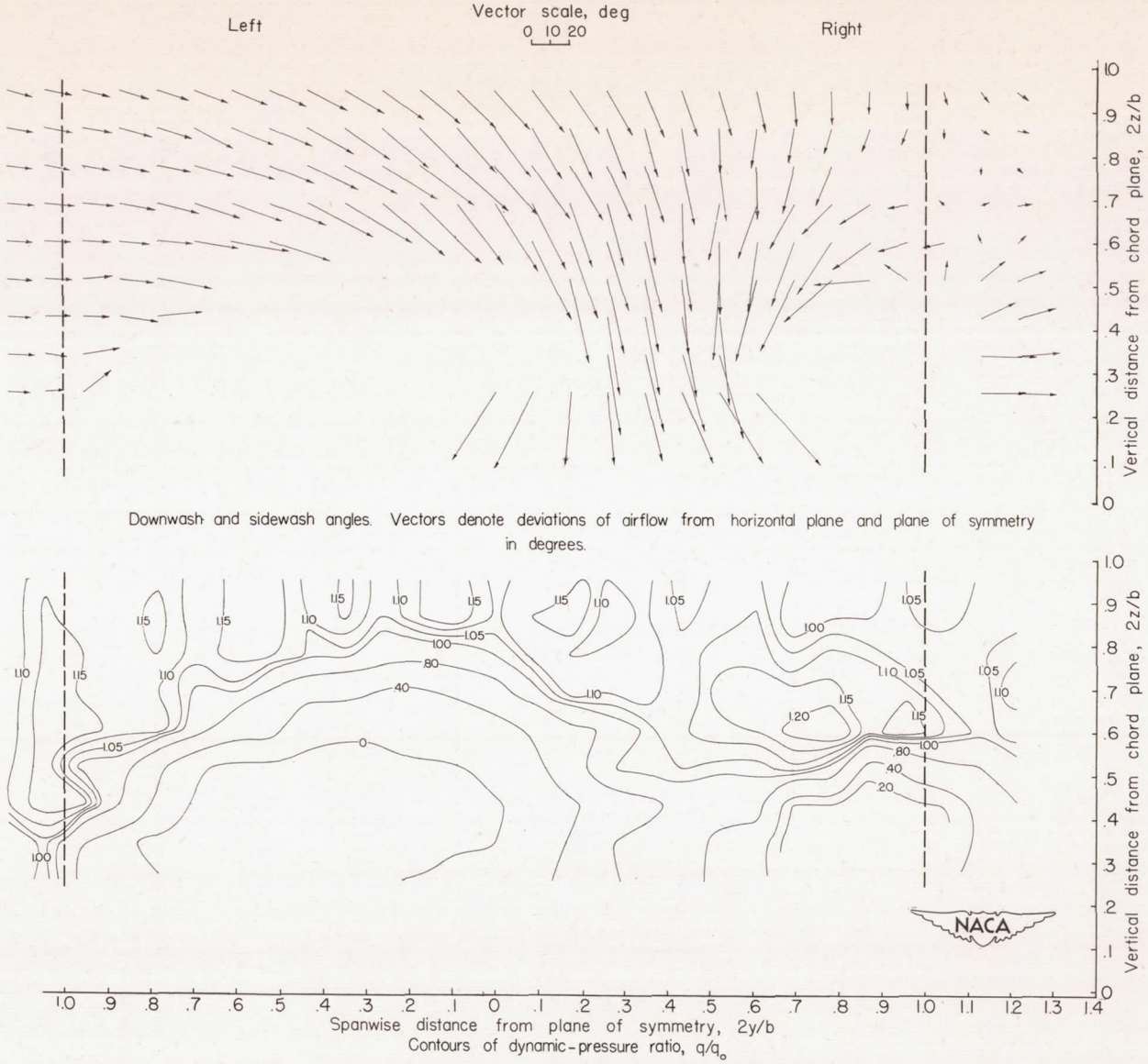

(e) $C_L = 0.90$; $\alpha = 28.0^{\circ}$.

Figure 10.- Concluded.

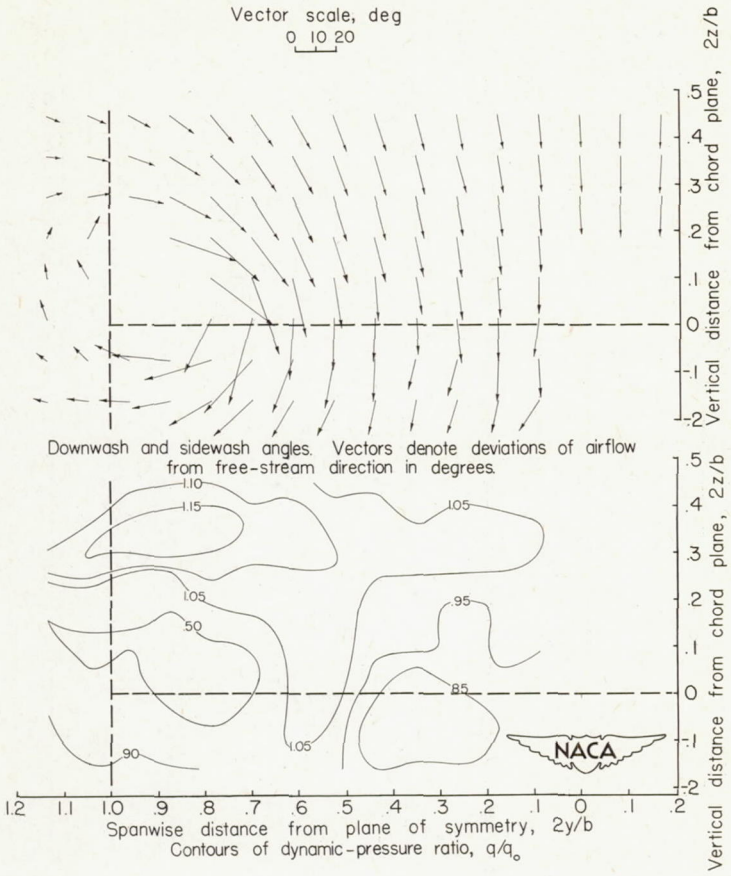

(a) $C_L = 0.86$; $\alpha = 10.1^{\circ}$.

Figure 11.- Vectors of downwash and sidewash and contours of dynamic-pressure ratio behind a 60° triangular wing. Longitudinal plane of survey at $1.05\bar{c}$ back of $\bar{c}/4$. Configuration A; $\psi = 0^{\circ}$; $\delta_f = 20^{\circ}$.

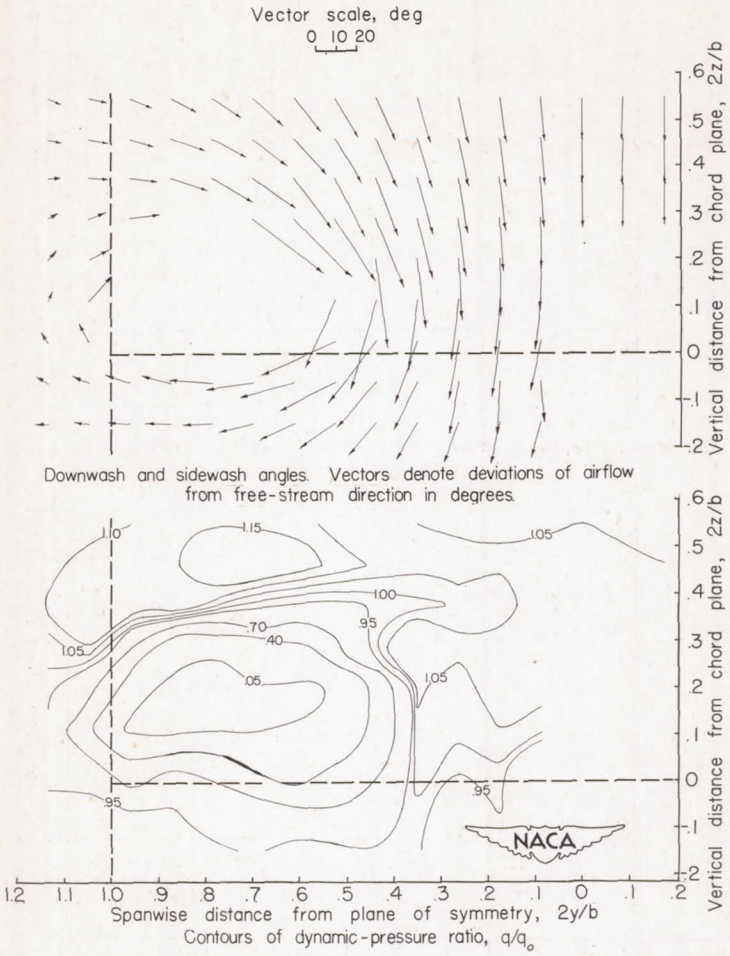

(b) $C_L = 0.93$; $\alpha = 15.9^{\circ}$.

Figure 11.- Continued.

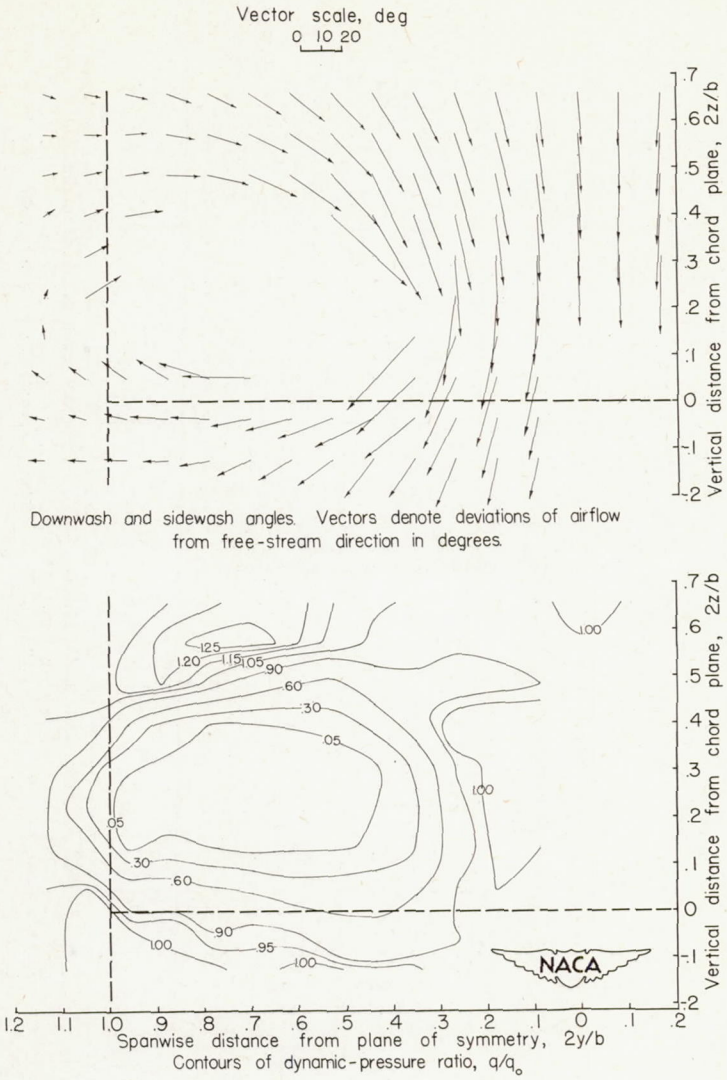

(c) $C_L = 1.06$; $\alpha = 21.6^{\circ}$.

Figure 11.- Concluded.

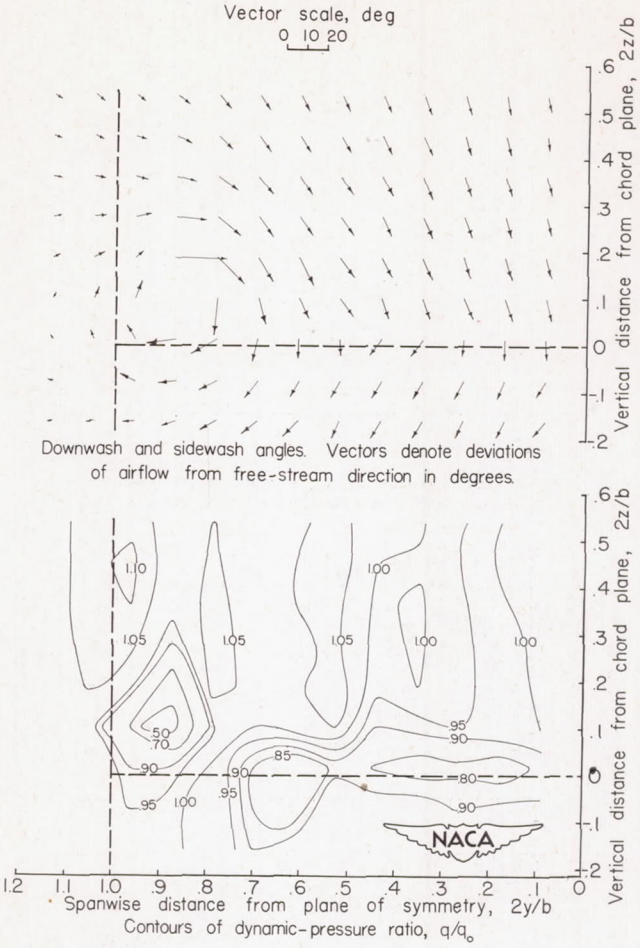

(a) $C_L = 0.43$; $\alpha = 11.2^{\circ}$.

Figure 12.- Vectors of downwash and sidewash and contours of dynamic-pressure ratio behind a 60° triangular wing. Longitudinal plane of survey at $1.05\bar{c}$ back of $\bar{c}/4$. Configuration B; $\psi = 0^{\circ}$; $\delta_f = 0^{\circ}$.

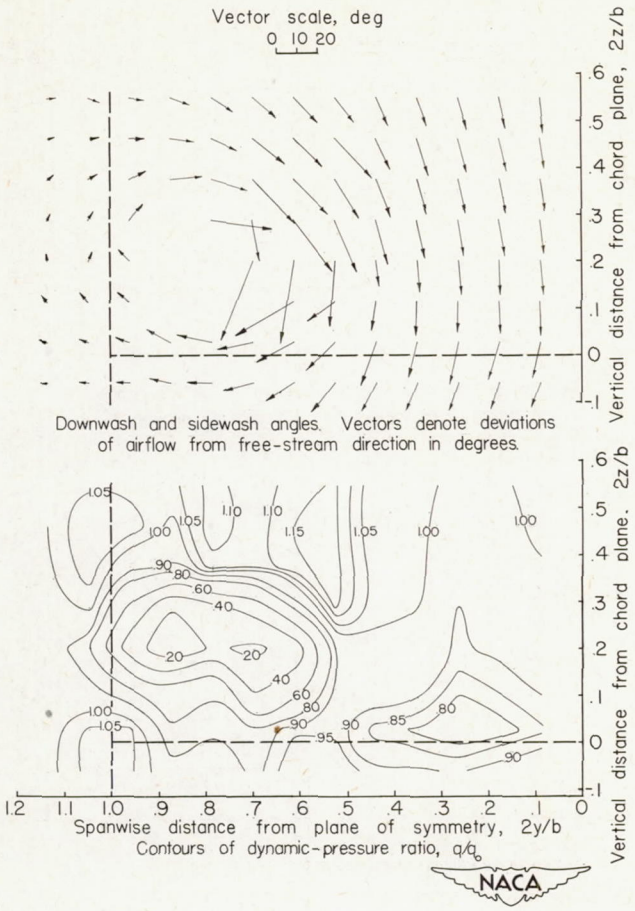

(b) $C_L = 0.67$; $\alpha = 16.5^{\circ}$.

Figure 12.- Continued.

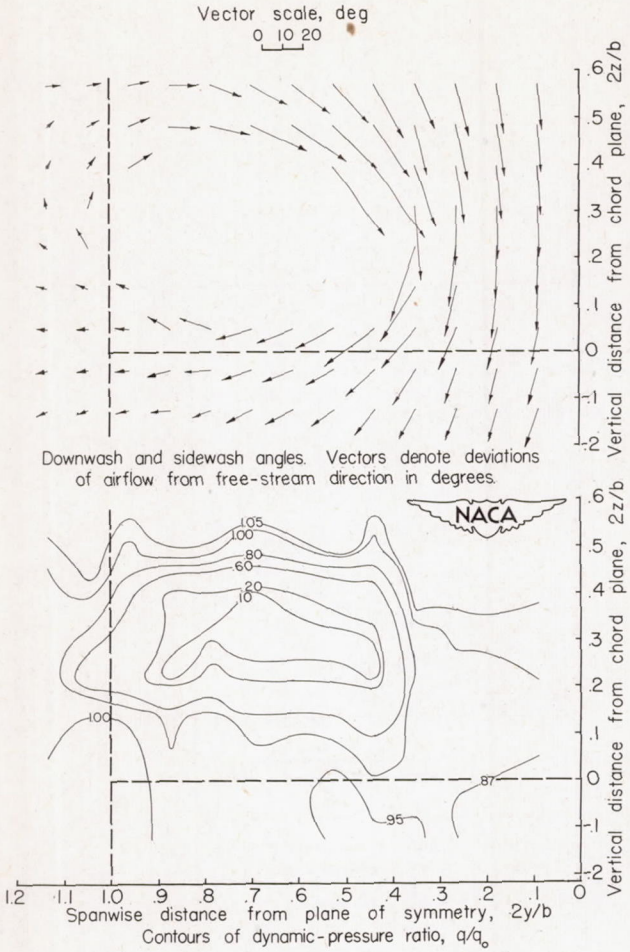

(c) $C_L = 0.84$; $\alpha = 22.1^{\circ}$.

Figure 12.- Concluded.

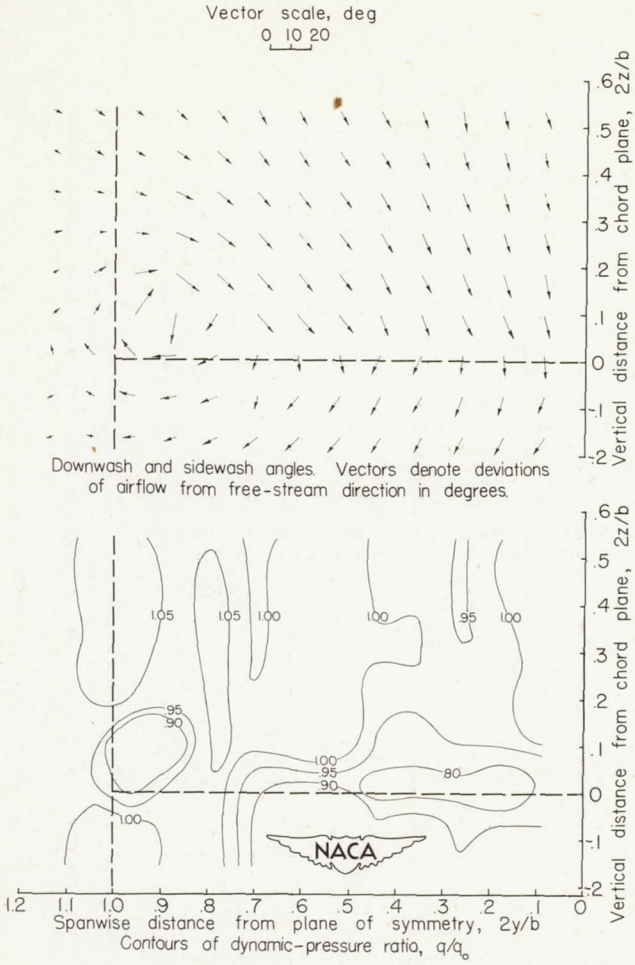

(a) $C_L = 0.42$; $\alpha = 11.1^{\circ}$.

Figure 13.- Vectors of downwash and sidewash and contours of dynamic-pressure ratio behind a 60° triangular wing. Longitudinal plane of survey at $1.05\bar{c}$ back of $\bar{c}/4$. Configuration C; $\psi = 0^{\circ}$; $\delta_f = 0^{\circ}$.

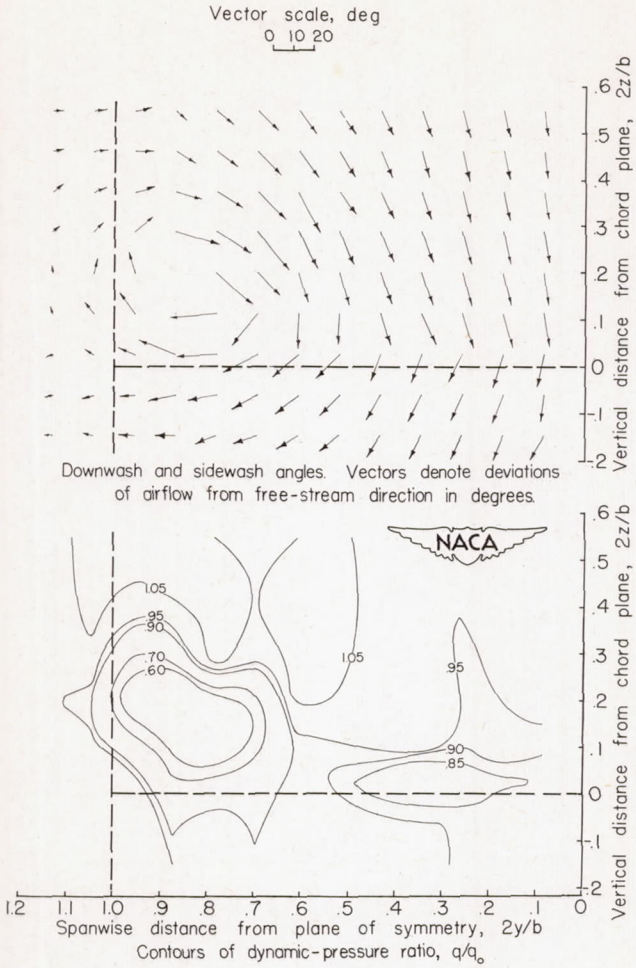

(b) $C_L = 0.62$; $\alpha = 16.5^{\circ}$.

Figure 13.- Continued.

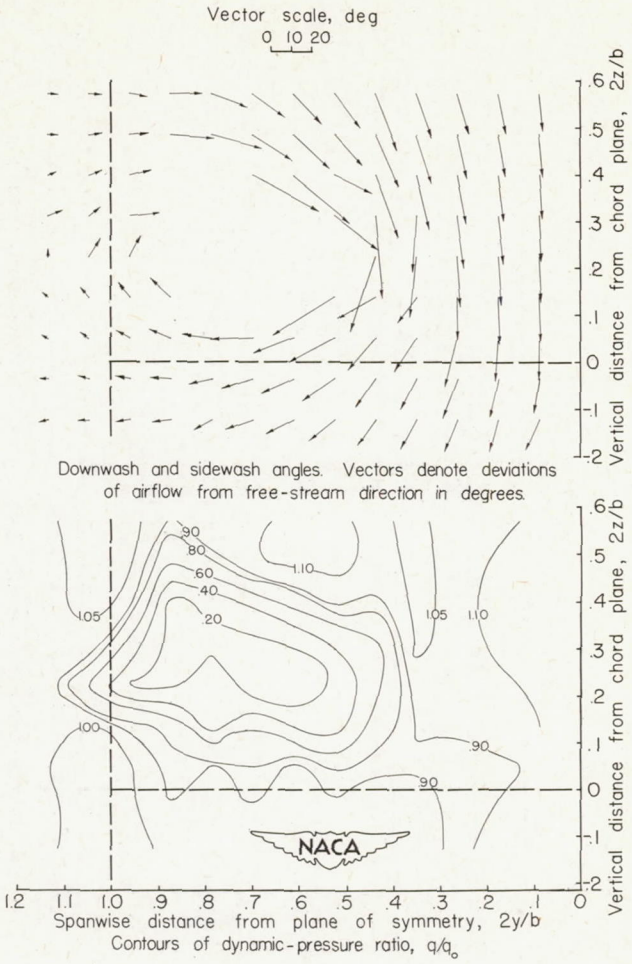

(c) $C_L = 0.80$; $\alpha = 22.1^{\circ}$.

Figure 13.- Concluded.

	S_t/S	l_1	l_2
S_{t_1}	0.1	$0.67\bar{c}$	$1.38\bar{c}$
S_{t_2}	0.2	$0.73\bar{c}$	$1.44\bar{c}$
S_{t_3}	0.3	$0.78\bar{c}$	$1.49\bar{c}$

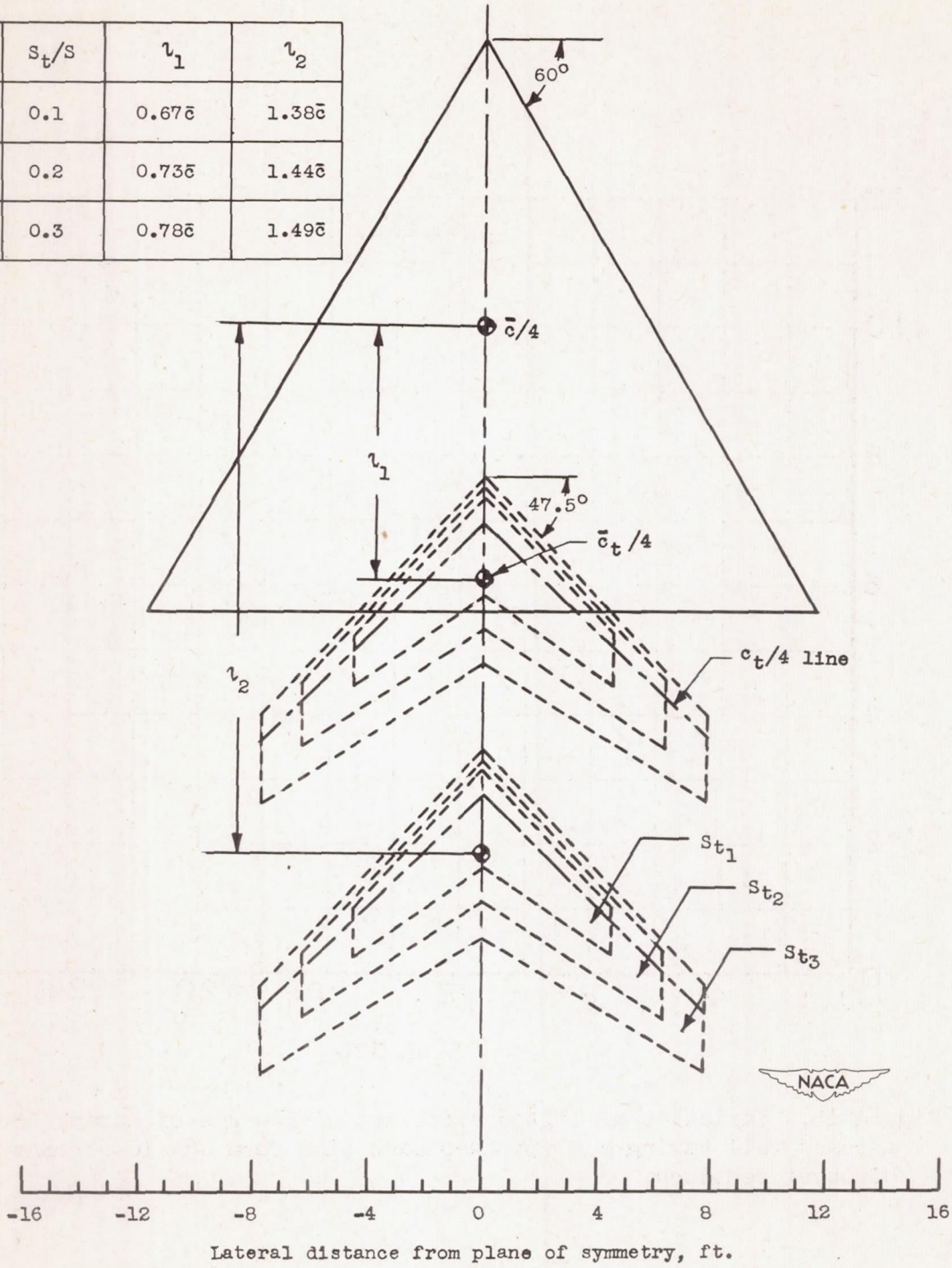

Figure 14.- Longitudinal locations of the assumed horizontal tails.

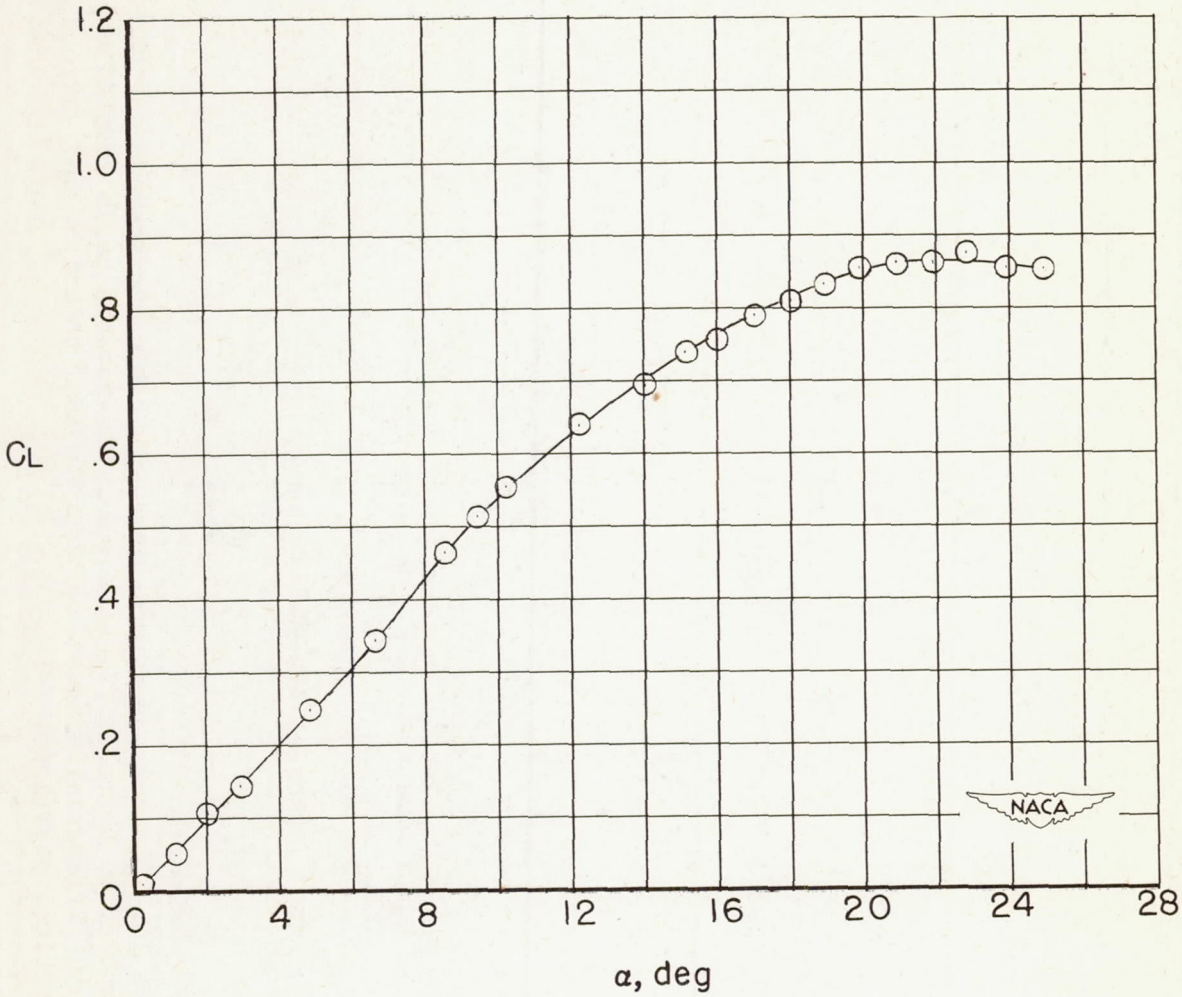

Figure 15.- Variation of lift coefficient with angle of attack for the assumed tail having a 47.5° sweptback plan form and 10-percent-thick biconvex sections.

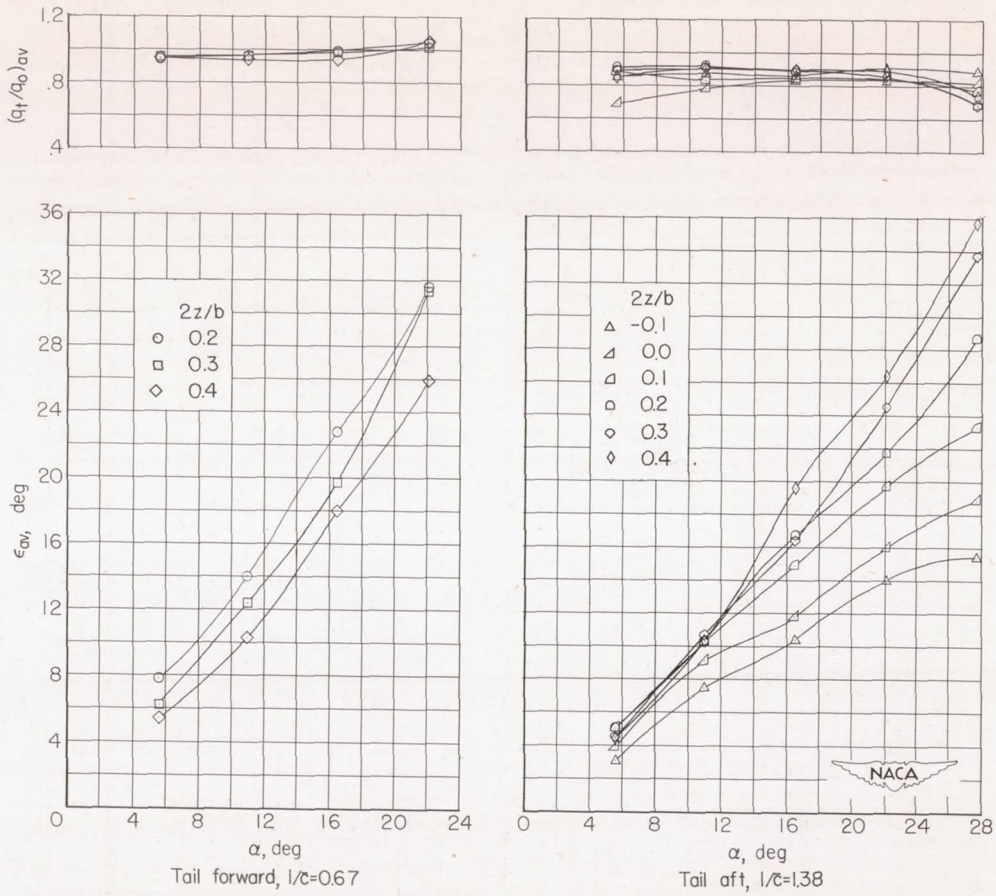

(a) $\frac{S_t}{S} = 0.1.$

Figure 16.- The average dynamic-pressure ratio and average downwash imposed on three different assumed all-movable tails located behind a 60° triangular wing at two longitudinal positions and various vertical positions.

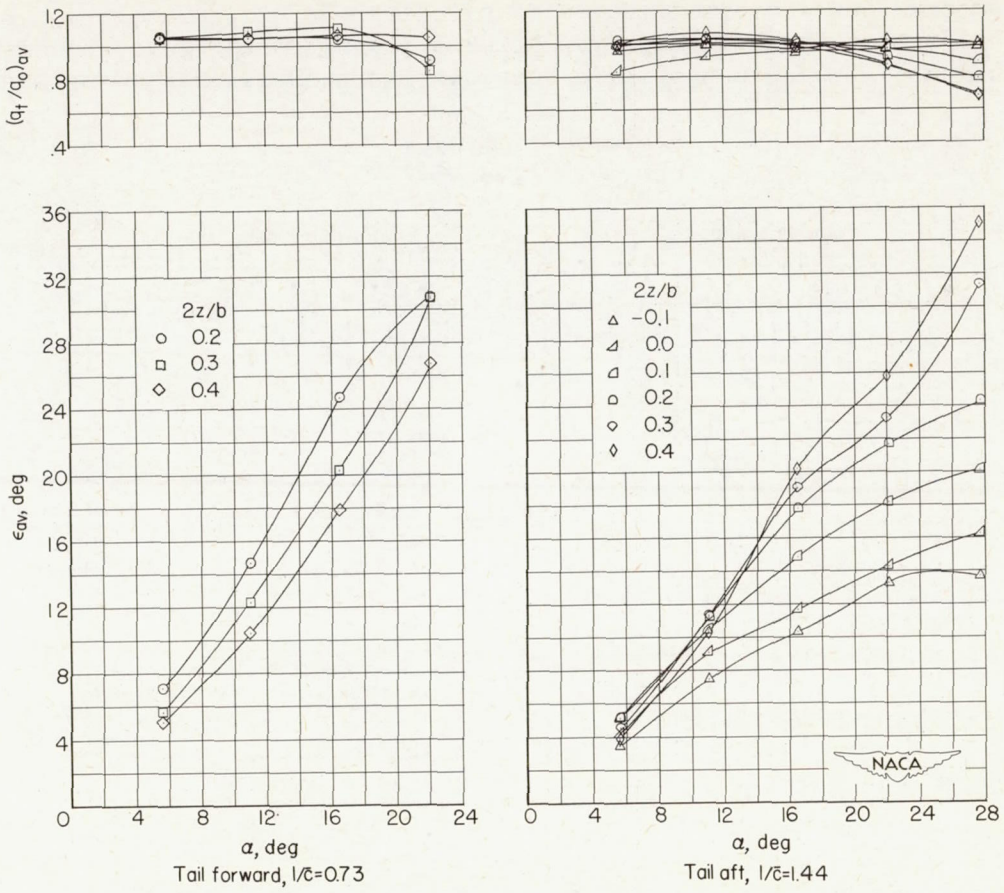

(b) $\frac{S_t}{S} = 0.2.$

Figure 16.- Continued.

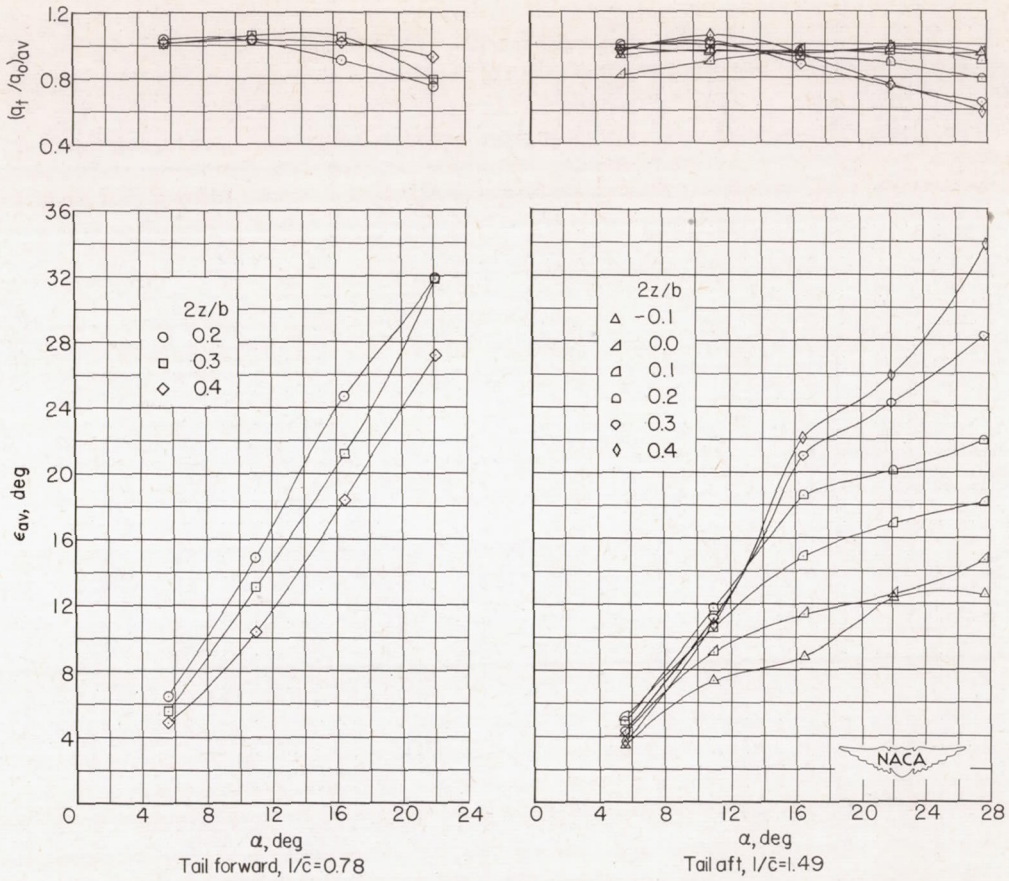

(c) $\frac{S_t}{S} = 0.3.$

Figure 16.- Concluded.

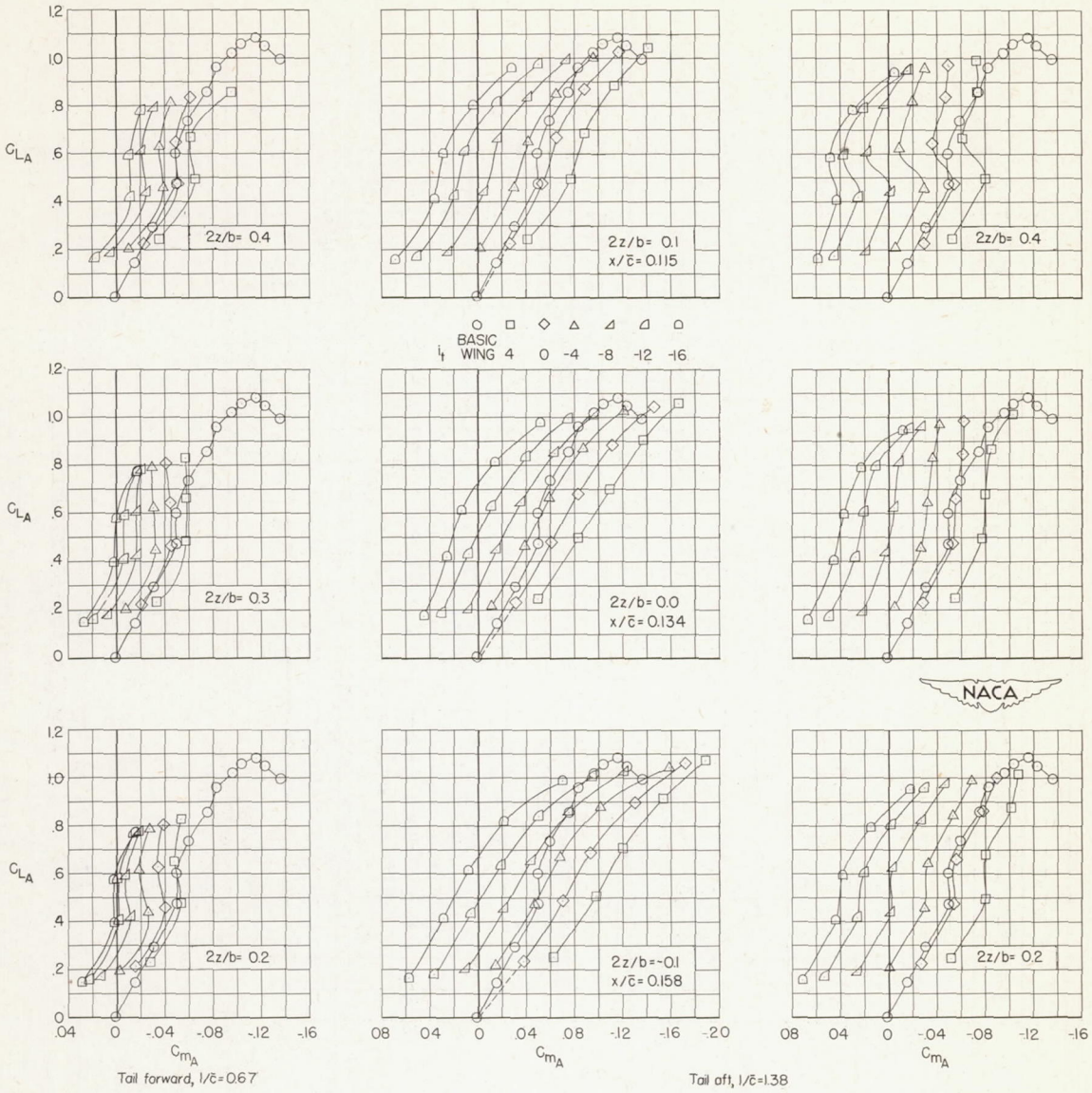

(a) $\frac{S_t}{S} = 0.1.$

Figure 17.- The static longitudinal stability characteristics of a 60° triangular-wing airplane with three assumed all-movable horizontal tails at two longitudinal positions and various vertical positions. The center of gravity is located at 0.25$\bar{c}$.

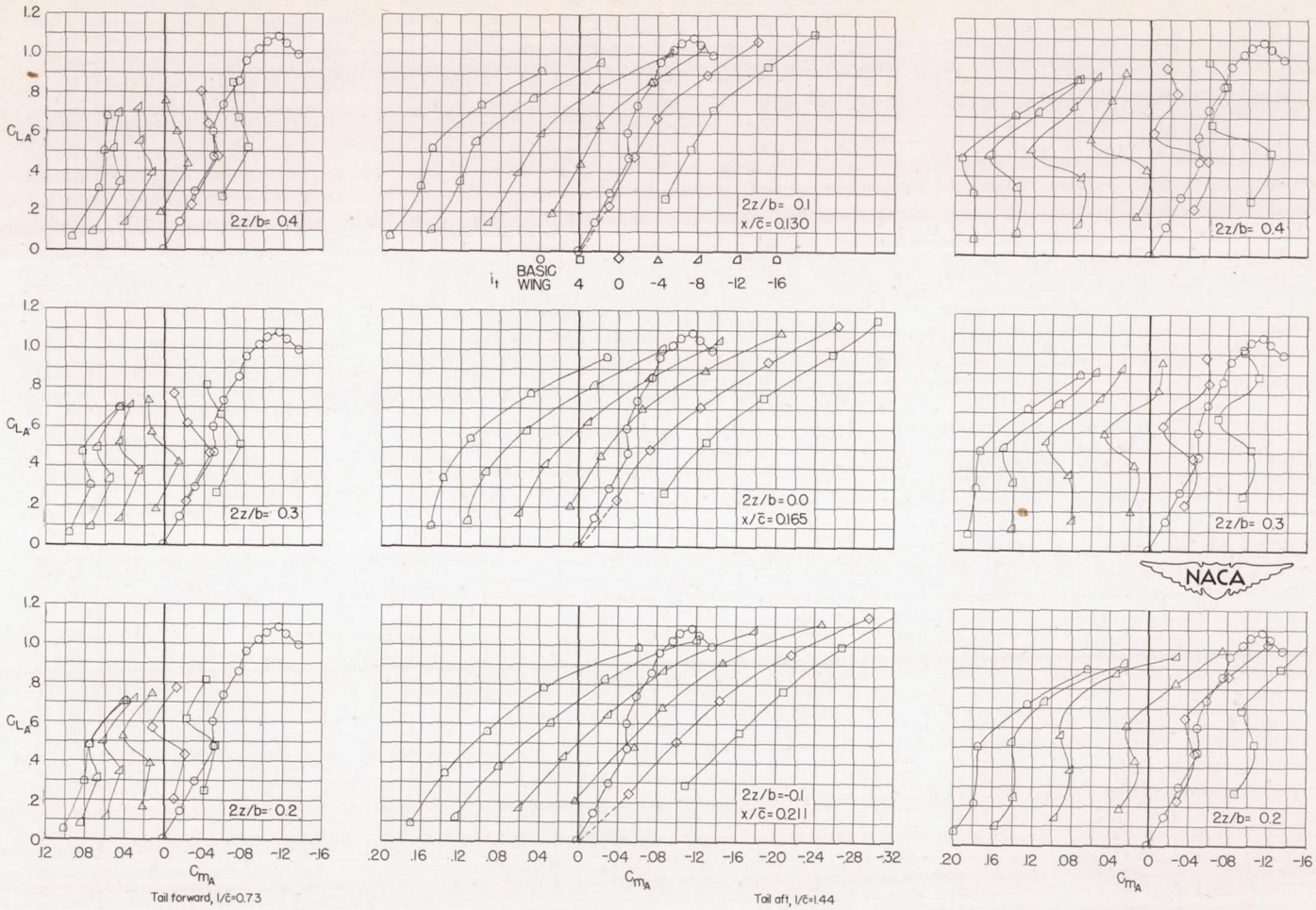

(b) $\frac{S_t}{S} = 0.2.$

Figure 17.- Continued.

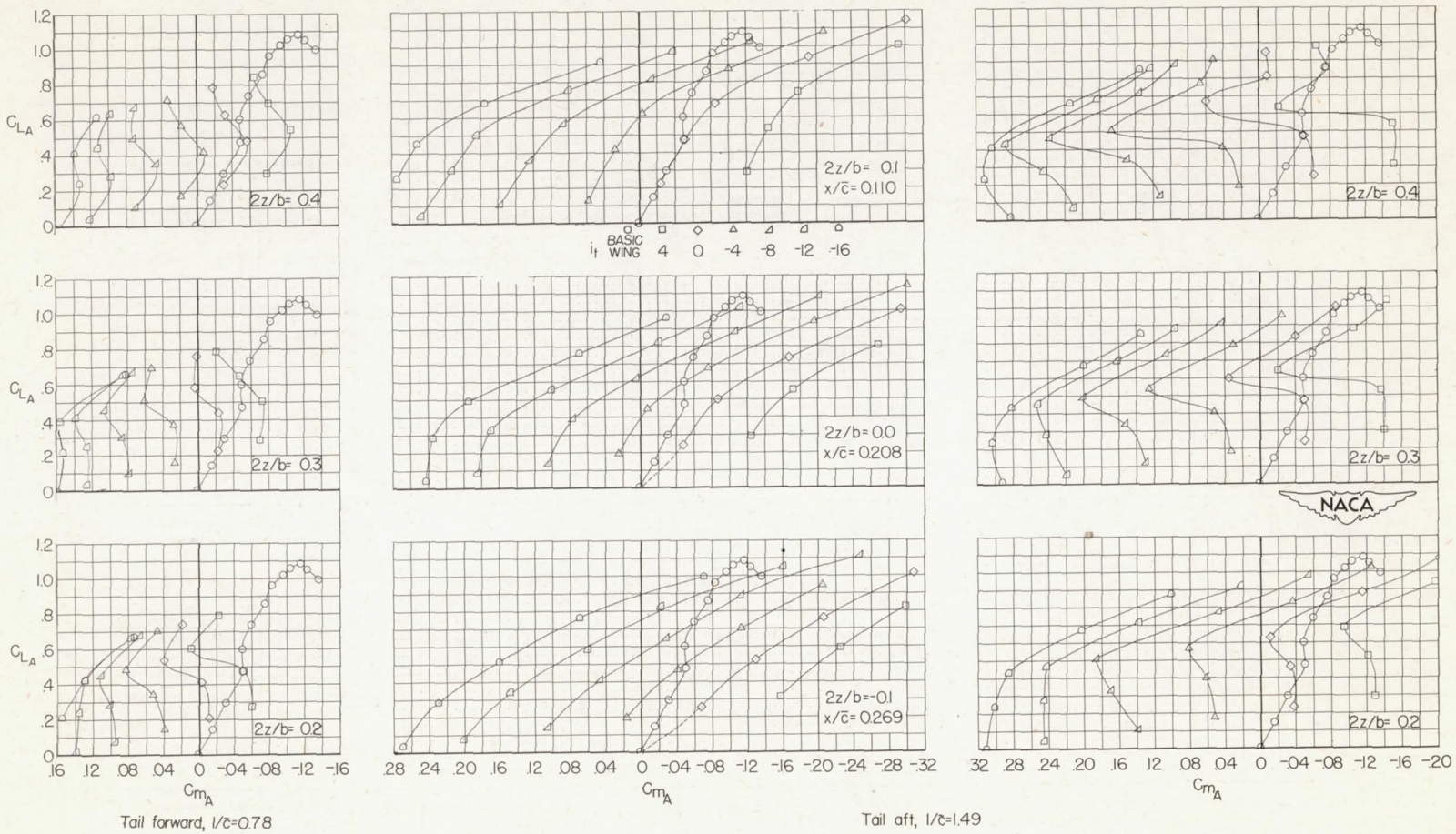

(c) $\frac{S_t}{S} = 0.3.$

Figure 17.- Concluded.

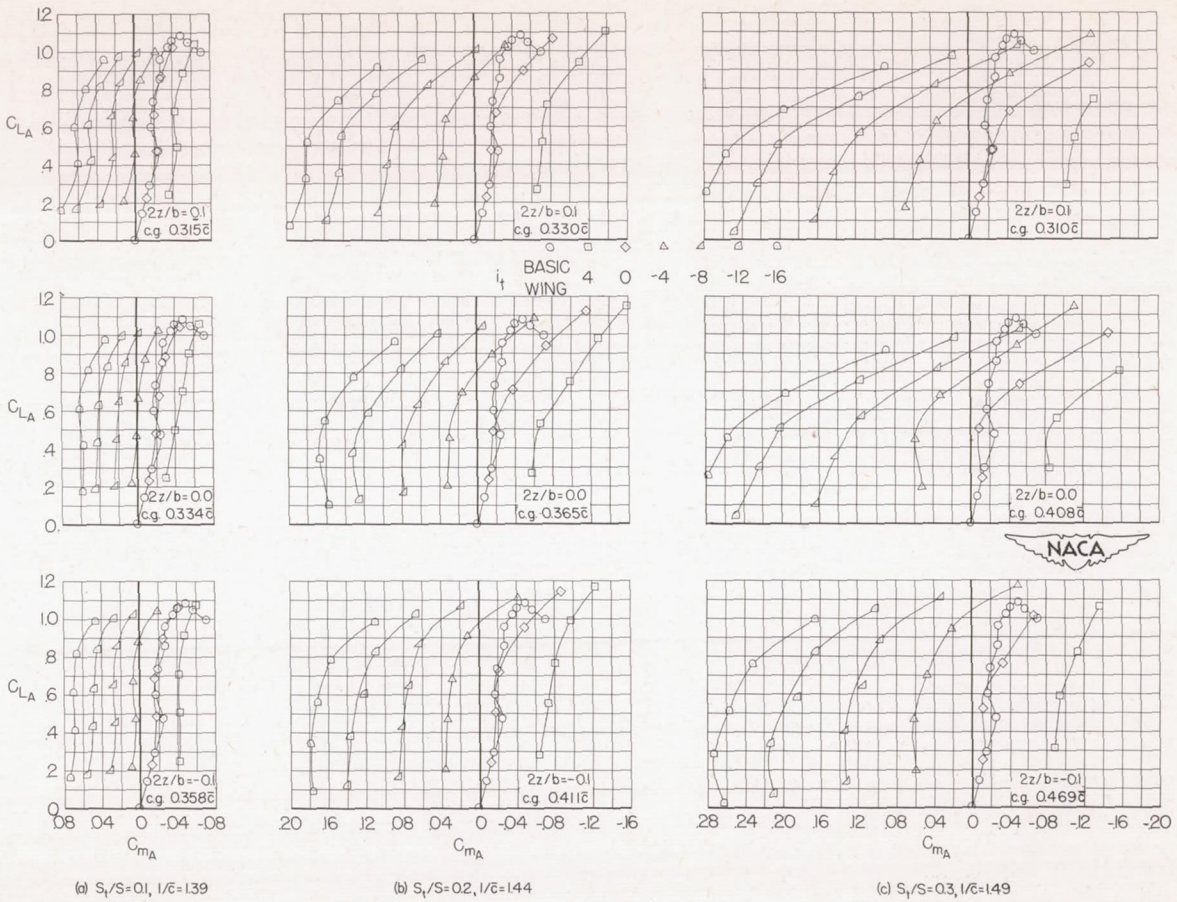

(a) $S_t/S=0.1$, $l/\bar{c}=1.39$ (b) $S_t/S=0.2$, $l/\bar{c}=1.44$ (c) $S_t/S=0.3$, $l/\bar{c}=1.49$

Figure 18.- The static longitudinal stability characteristics of a 60° triangular-wing airplane having three different assumed all-movable horizontal tails located at a representative aft location and three vertical positions and having a static margin $(x/\bar{c})_{C_L=0}$ of 0.05 at $i_t = 0°$.

NACA-Langley - 10-27-52 - 350